Electrochimica Acta 555 (2026) 148353

Contents lists available at ScienceDirect

Electrochimica Acta

journal homepage: www.journals.elsevier.com/electrochimica-acta

3D-printed electrochemical cell for both detection and degradation of venlafaxine and desvenlafaxine with boron-doped diamond electrode

Martin Šefčík [a], Ghazaleh Kholafazadehastamal [a], Thomas Peeters [b], Jan Fischer [a], Anna Kubíčková [a], Clive E. Hall [c], Josephus G. Buijnsters [b,*], Simona Baluchová [a,*]

[a] Department of Analytical Chemistry, Faculty of Science, Charles University, Albertov 6, 128 00 Prague, Czech Republic
[b] Department of Precision and Microsystems Engineering, Faculty of Mechanical Engineering, Delft University of Technology, Mekelweg 2, 2628 CD Delft, the Netherlands
[c] Mintres BV, De Nieuwe Erven 8, 5431 NT Cuijk, the Netherlands

ARTICLE INFO

Keywords:
3D-printed electrochemical cell
Boron-doped diamond (BDD)
Electroanalysis
Venlafaxine
Desvenlafaxine
Electrochemical degradation

ABSTRACT

Venlafaxine (VF) and its active metabolite desvenlafaxine (DVF) are widely prescribed antidepressants that are only partially metabolized and excreted in significant amounts, making them clinically important analytes and environmentally relevant contaminants. In this study, a free-standing boron-doped diamond (BDD) electrode is exploited in a dual role for the electrochemical detection and degradation of VF and DVF, integrated into a custom 3D-printed dual-function electrochemical cell. The nucleation (BDD_{NS}) and growth (BDD_{GS}) sides of the BDD plate were systematically compared under different surface terminations. Oxidized BDD_{NS} (O-BDD_{NS}) provided three well-resolved oxidation peaks for VF, whereas hydrogen-terminated BDD_{NS} (H-BDD_{NS}) yielded a single distinct peak for DVF in 0.1 M H_2SO_4. Differential pulse voltammetric (DPV) methods were developed with limits of detection of 0.35 μM for VF (peak 1) and 0.34 μM for DVF and wide linear ranges in the low-to-high micromolar region. By exploiting the different surface-termination preferences and multi-peak behaviour of VF, simultaneous determination of VF and DVF was achieved. The methods showed good selectivity toward common interferents and were successfully applied to spiked river water and pharmaceutical capsules using the standard addition approach, giving recoveries close to 100 %. In the 3D-printed cell, BDD_{GS} was used for electrochemical advanced oxidation, achieving ~97 % degradation of 1 mM VF and DVF in 0.1 M H_2SO_4 within 20 min under galvanostatic conditions, following pseudo-first-order kinetics. In situ DPV on BDD_{NS} enabled real-time monitoring of VF decay, demonstrating an integrated detect-and-degrade platform based on BDD and additive manufacturing.

1. Introduction

Depression is a major global health disorder, affecting hundreds of millions of people worldwide [1] and driving widespread use of the antidepressants venlafaxine (VF) and its active metabolite desvenlafaxine (DVF), both serotonin–norepinephrine reuptake inhibitors [2]. However, both compounds are only partially metabolized and are excreted in significant amounts – up to 5 % as unchanged VF, 29 % as DVF from VF metabolism [3], and 45 % as unchanged DVF [4] – leading to their accumulation in wastewaters [5–7] and natural waters [8].

Both VF and DVF are persistent, poorly degradable, and toxic to aquatic organisms [9,10]. They have been detected globally in surface waters at concerning levels [8,11] and, due to their ecotoxicological risk, are included on the European Union's Surface Water Watch List under the Water Framework Directive [9]. Conventional wastewater treatment processes achieve only limited removal efficiency [7,12], with one study reporting VF removal of approximately 40 % [13]. Their persistence highlights the urgent need for reliable monitoring strategies for not only clinical but also for environmental matrices.

Conventional analytical techniques for VF and DVF, such as high-performance liquid chromatography (HPLC) coupled with mass spectrometry (HPLC-MS/MS), provide high sensitivity and selectivity [2,14]. However, these methods require expensive instrumentation, labour-intensive sample preparation, and trained personnel, which limits their applicability for rapid or on-site monitoring. In contrast, electrochemical detection offers a cost-effective, reliable, accurate, portable, and straightforward alternative.

Electrochemical sensing represents a promising approach for the

* Corresponding authors.
E-mail addresses: j.g.buijnsters@tudelft.nl (J.G. Buijnsters), simona.baluchova@natur.cuni.cz (S. Baluchová).

https://doi.org/10.1016/j.electacta.2026.148353
Received 21 December 2025; Received in revised form 28 January 2026; Accepted 31 January 2026
Available online 1 February 2026

detection of VF and DVF [15,16]. To date, the majority of studies have employed sp^2-carbon-based electrodes, such as carbon paste [17], glassy carbon [18], and screen-printed carbon [19,20] electrodes; see Table S1 in Supplementary Material for a more extensive overview of electrochemical sensors developed for VF and DVF detection so far. However, in most cases, bare sp^2-carbon surfaces failed to yield analytically useful signals, necessitating surface modification. Common modifiers include multi-walled carbon nanotubes [17,18] and inorganic nanoparticles such as ZnO [17], Gd_2O_3 [20], and Co_3O_4 [19], used individually or in combination. These modification procedures are typically multi-step, time-consuming, and complex. Moreover, issues with stability and reproducibility in electrode fabrication can negatively impact the reliability and consistency of the analytical results.

Among electrode materials, the sp^3-carbon-based boron-doped diamond (BDD) has emerged as particularly attractive due to its exceptional chemical stability, low background currents, wide potential window, high signal-to-noise ratio, and strong resistance to surface fouling [21,22]. These properties collectively contribute to the long-term reliability and stability of BDD electrodes in electrochemical applications. However, it should be pointed out that the electrochemical performance of BDD electrodes is strongly influenced by a range of parameters [21,22], including boron doping level [23,24], surface termination [25–27], sp^2-carbon content [28], and crystallographic orientation [25,27].

BDD electrodes can be fabricated either as thin films (with thicknesses of several hundred nanometres) deposited on substrates such as silicon, titanium, or as free-standing thick plates (with thicknesses of several hundred micrometres) [22]. In the case of BDD thin films, only the growth surface is accessible for electrochemical measurements, whereas free-standing BDD typically provides both nucleation and growth faces, which may be used either in their as-deposited or polished state. We have previously demonstrated that nucleation, growth, and polished growth surfaces differ markedly in grain size, boron dopant distribution, and sp^2-carbon content [28,29], which translates into distinct electrochemical behaviour, for example in glucose sensing [28] and electrochemical degradation of carbamazepine in water treatment [30].

In electroanalysis, BDD electrodes have been successfully applied to the detection of various pharmaceuticals [21,26,31–34]. To the best of our knowledge, only one study to date has reported the use of a commercially available, unmodified BDD thin-film electrode for VF detection [35], employing batch injection analysis with amperometric detection as the main analytical approach.

Beyond detection, the removal of VF and DVF from aquatic environments is a growing concern. Electrochemical advanced oxidation processes (EAOPs) have gained attention as green technologies for the degradation of persistent pollutants [36–38]. BDD electrodes are particularly well-suited for such applications due to their high oxygen evolution overpotential, which enables the efficient generation of hydroxyl radicals with strong oxidizing capabilities [39–42]. As in sensing applications, the performance of BDD in EAOPs is influenced by key material properties such as boron doping level, grain size, and the density of grain boundaries containing non-diamond (sp^2) carbon [30,43–45]. These factors collectively affect the generation of reactive radical species, and thus directly impact the degradation kinetics and overall removal efficiency of organic contaminants, including VF [44]. BDD electrodes have already been successfully applied to the degradation of VF in lab-made solutions [46] as well as in real wastewater [44], while in the latter 100 % removal efficiency, monitored through HPLC-UV/MS, was achieved within 4 h under optimized BDD synthesis and operating conditions.

In parallel, additive manufacturing has recently expanded the design possibilities of electrochemical systems. 3D printing enables the fabrication of custom-made, low-cost, and reproducible devices with tailored geometries and integrated functionalities [47–50]. Tailored 3D-printed electrochemical cells have been designed to optimize reactor geometry and flow configuration for specific processes, improving control over mass transport and operating conditions [47]. Complete additively manufactured sensing platforms have also been demonstrated, in which both the cell body and electrode components are printed yet still provide robust analytical performance [48]. Furthermore, 3D-printed architectures have been used to integrate microfluidic channels with impedimetric sensing elements in compact devices [49], and to construct filter-press electrochemical reactors that offer a versatile, low-cost option for multipurpose laboratory applications [50].

In this work, we present a comprehensive and methodologically novel electrochemical strategy to address the challenges associated with the detection and degradation of VF and DVF using a free-standing BDD plate. First, we evaluate both sides of the free-standing BDD electrode to identify the most suitable surface, along with the optimal surface termination (H- vs. O-) that promotes signal development. Second, we develop and optimize electroanalytical methods for the detection of VF and DVF, and demonstrate their applicability through analyses of river water and pharmaceutical capsule samples. Ultimately, we employ the same free-standing BDD electrode for the electrochemical degradation of VF and DVF, and introduce a custom-designed 3D-printed electrochemical cell that enables the integrated detection and degradation of these two antidepressants. To the best of our knowledge, this is the first report combining side-selective use of a free-standing BDD electrode with a 3D-printed dual-function cell for simultaneous electroanalytical monitoring and electrochemical degradation of antidepressants.

2. Experimental

2.1. Reagents and solutions

Analytical reagent grade chemicals were obtained from Sigma-Aldrich and used as-received: venlafaxine hydrochloride, *O*-desmethylvenlafaxine, potassium hexacyanoferrate(II) trihydrate, sulphuric acid (97 %), *ortho*-phosphoric acid (85 %), potassium nitrate, acetic acid, boric acid, sodium hydroxide, phosphate buffered saline (PBS; tablets, pH 7.4), glucose, sucrose, ascorbic acid, citric acid, dopamine, and acetonitrile. Olwexya® (venlafaxine hydrochloride, 150 mg) commercial capsules were purchased from KRKA Co., Czech Republic.

Stock solutions of VF and DVF (1.0 mM) were prepared in deionized water or a 1:1 mixture of deionized water and acetonitrile, respectively, and stored in the dark at 4 ± 1 °C. Universal Britton–Robinson (BR) buffers (0.04 M) with pH ranging from 2.0 to 12.0 were prepared by mixing the acidic component (a combination of *ortho*-phosphoric, acetic, and boric acids) with 0.2 M sodium hydroxide to adjust the pH, which was measured using a Metrohm 913 pH meter.

All aqueous solutions were made using ultra-pure water (resistivity of >18.0 MΩ cm), purified with a LWTN Genie A system (Laboratorium Water Technologie Nederland).

2.2. Instrumentation and procedures

2.2.1. Electroanalytical measurements

All electroanalytical measurements were performed at laboratory temperature (23 ± 1 °C) using an Autolab PGSTAT128N controlled by Nova 2.1 software (Metrohm, the Netherlands). A conventional three-electrode configuration was employed, consisting of a free-standing BDD electrode (Mintres, the Netherlands) as the working electrode, a silver-silver chloride electrode (Ag|AgCl|3 M NaCl) as the reference electrode, and a platinum wire (both provided by Bio-Logic, France) as the counter electrode. The free-standing BDD electrode (1.5 × 1.5 cm^2), approximately 300 μm thick and with average boron doping level of 3×10^{20} atoms cm^{-3}, featured both the nucleation side (BDD_{NS}) and the growth side (BDD_{GS}), each mechanically polished and available for electrochemical measurements. During electroanalytical experiments, the BDD electrode was mounted at the bottom of an electrochemical cell such that only one side (either BDD_{NS} or BDD_{GS}) was exposed to the solution through a circular aperture (5 mm diameter), thereby defining

the active working area. Comprehensive morphological and structural characterization of BDD_{NS} and BDD_{GS} surfaces, including scanning electron microscopy, atomic force microscopy, and Raman spectroscopy (spectra and mapping), has been reported previously in [28–30].

2.2.2. BDD surface pre-treatments

Two surface terminations of the BDD electrode were investigated: an oxygen-terminated (O-BDD) and a hydrogen-terminated (H-BDD) surface for both the BDD_{NS} and BDD_{GS} electrode sides. Surface termination was modified electrochemically using two distinct pre-treatment procedures carried out in 0.1 M H_2SO_4. For anodic oxidation, a potential of +2.4 V was applied for 20 min to produce an oxygen-enriched surface, while cathodic hydrogenation was achieved by applying –2.4 V for 20 min to generate a hydrogen-enriched surface. Between individual measurements, a shorter reactivation step (30 s at the respective potential) was employed to maintain surface termination. The effectiveness of each pre-treatment method was evaluated using a 1 mM $[Fe(CN)_6]^{3-/4-}$ redox probe, which is sensitive to the nature of the surface functional groups [25,51].

2.2.3. Optimization of DPV parameters

Differential pulse voltammetric (DPV) parameters, i.e., pulse amplitude (A), pulse width (t), and potential step (E_s), were independently optimized for VF (at O-BDD_{NS}) and DVF (at H-BDD_{NS}), both at 100 μM concentration. Each parameter was varied within the ranges A: 10–150 mV (VF) / 10–250 mV (DVF), t: 5–50 ms, and E_s: 5–25 mV, while keeping the others constant. The final optimized conditions were: (i) VF at O-BDD_{NS}: $A = 115$ mV, $t = 10$ ms, $E_s = 15$ mV; (ii) DVF at H-BDD_{NS}: $A = 200$ mV, $t = 20$ ms, $E_s = 15$ mV. Prior to optimization, particularly for the pH study, the used DPV parameters for both compounds were $A = 60$ mV, $t = 50$ ms, and $E_s = 15$ mV.

2.3. Analytical performance

Using the optimized DPV parameters, calibration curves for VF on O-BDD_{NS} and DVF on H-BDD_{NS} were constructed from the average of four replicate measurements per calibration solution. Linear regression was applied using the least squares method. The limits of detection (LOD) and quantification (LOQ) were calculated as three and ten times the standard deviation ($n = 10$) of the peak current at the lowest measurable concentration, respectively, divided by the slope of the corresponding calibration curve.

Simultaneous determination of VF and DVF was also investigated using DPV under the optimized parameters described above. Three calibration protocols were employed: (1) dual-variation calibration, where VF and DVF were present together and varied simultaneously from 1.0 to 10.0 μM (O-BDD_{NS}); (2) selective calibration for VF, where DVF was kept constant at 5.0 μM and VF was varied from 1.0 to 14.0 μM (O-BDD_{NS}); and (3) selective calibration for DVF, where VF was fixed at 10.0 μM and DVF was varied from 4.0 to 20.0 μM (H-BDD_{NS}). For each protocol, calibration curves were constructed and LOD and LOQ values were calculated using the same procedure as described above.

2.4. Interference study

The selectivity of the developed DPV methods was evaluated by introducing potential interfering compounds. Sugars (glucose, sucrose) were tested at a 500-fold excess, while ascorbic acid, citric acid, and dopamine were added at analyte-to-interferent ratios of 1:1, 1:10, 1:25, 1:50, and 1:100. The influence on the VF and DVF signals (10.0 μM) was assessed, and interference was considered negligible if the peak current deviated by less than ±10 % compared to the signal obtained in the absence of interferents.

2.5. Real samples analysis

A 250 mL river water sample was collected from the Schie River (Delft, the Netherlands), filtered to remove particulate matter, and used without further treatment. Aliquots were spiked with 50.0 μM VF or DVF and subsequently diluted with 0.1 M H_2SO_4 in a 1:9 (v/v) ratio, resulting in a final analyte concentration of 5.0 μM. The standard addition method was applied using two additions (100 μL each) of a 1.0 mM VF or DVF stock solution. VF was determined on O-BDD_{NS} and DVF on H-BDD_{NS}, and all measurements were performed in triplicate ($n = 3$) to account for matrix effects and enable accurate quantification.

Pharmaceutical venlafaxine capsules were analysed using three commercial units, each labelled to contain 150 mg VF. Capsules were carefully opened, and shells and contents were weighed separately. An accurately weighed portion of the fill material, corresponding to a final VF concentration of 5.0 mM in 100 mL, was transferred to a volumetric flask. Sample preparation followed the relevant pharmacopeia procedure: 8 mL of acetonitrile (8 % of the final volume) was added and the mixture shaken for 40 min, followed by addition of 50 mL of an acetonitrile–deionized water mixture (25:75, v/v) and shaking for a further 20 min. The solution was then made up to 100 mL with the same acetonitrile–water mixture to obtain a 5.0 mM VF stock solution, which was filtered through a 0.45 μm membrane. Working solutions for DPV were prepared by dilution with 0.1 M H_2SO_4 to give VF concentrations of 10.0 μM, whereas a 0.20 mM VF solution was used for UHPLC-UV analysis. Standard addition (two to three aliquots of the VF stock solution) was applied in both DPV and UHPLC determinations, and each capsule extract was analysed in triplicate to correct for matrix effects and to evaluate method precision.

Chromatographic analysis of capsule extracts was carried out using an Ultra-High-Performance Liquid Chromatography (UHPLC) system Waters Acquity UPLC H—Class (Waters Corporation, Milford, MA, USA) equipped with a photodiode array detector ($\lambda = 224$ nm) and controlled by Empower 3 software. Analyses were performed on a Kinetex C18 column (1.7 μm, 100 × 2.1 mm) using gradient elution with acetonitrile and deionized water (10–50 % (v/v) acetonitrile in 5 min), both containing 0.1 % (v/v) formic acid, as the mobile phase.

2.6. Design, fabrication and validation of the 3D-printed cell

A custom 3D-printed dual-function electrochemical cell (internal volume of 12 mL), shown in Scheme 1, was developed for the oxidative degradation of VF and DVF and their subsequent detection by in situ voltammetry (using the optimized DPV parameters) and ex situ UHPLC-UV analysis. The cell was designed in Autodesk Fusion 360 (Autodesk Inc., USA) and fabricated on a Form 3 SLA printer (Formlabs, USA). The cell body, cover, presser, motor stand and stirrer were printed from Clear V4 resin, while sealing elements were printed from Silicone 40A resin. Clear V4 components were washed with isopropanol and post-cured for 30 min at 60 °C; Silicone 40A parts were cleaned in a 4:1 (v/v) isopropanol:*n*-butyl acetate mixture and post-cured in water for 45 min at 60 °C using a Form Cure unit (Formlabs, USA).

As depicted in Scheme 1 (and shown in Video S1), the free-standing BDD electrode was mounted vertically by inserting its lower edge into a triangular aperture and securing the upper edge with the cell cover. The nucleation side (BDD_{NS}) was oriented toward a stainless-steel wire electrode (0.5 mm diameter), which served as the counter electrode for voltammetric measurements, while the growth side (BDD_{GS}) faced a stainless-steel plate cathode (1.5 × 1.5 cm^2) used for electrochemical degradation. Thus, VF and DVF were degraded on the BDD_{GS}–stainless-steel plate anode-cathode pair (inter-electrode distance of 33 mm), whereas in situ DPV detection was always performed at the BDD_{NS} surface versus the stainless-steel wire counter electrode, with an Ag/AgCl reference electrode placed in close proximity to the BDD_{NS} surface. The wire counter electrode was installed in the back wall of the cell, and the plate cathode in the front wall, and both were sealed by clamping the

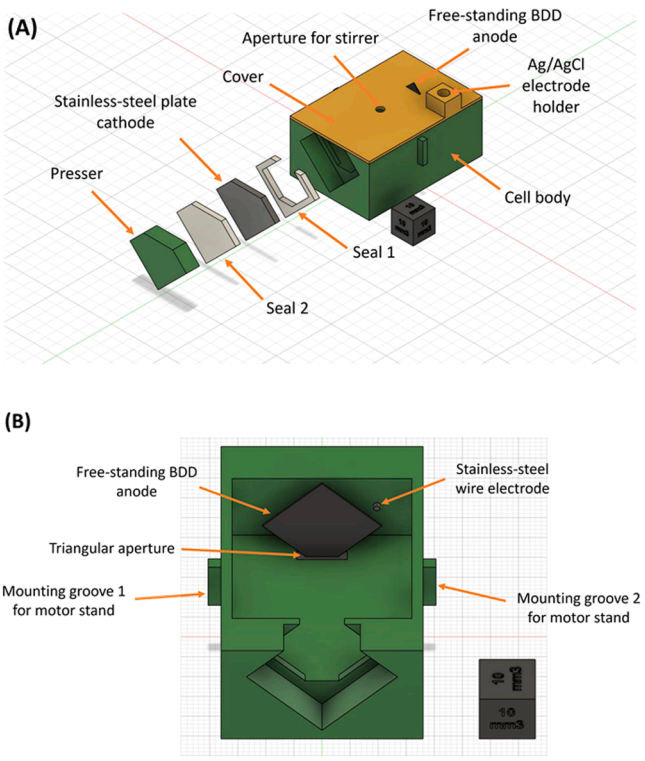

Scheme 1. Schematic representation of the 3D-printed dual-function electrochemical cell with labelled components, illustrating the arrangement of electrodes and structural elements: **(A)** external view, and **(B)** internal view.

presser and back wall together. Electrochemical degradation was carried out using a laboratory DC power supply (Owon, China), while in situ DPV measurements were performed with an Autolab PGSTAT128N (Metrohm, the Netherlands).

Degradation experiments of 1 mM VF and 1 mM DVF were conducted in 0.1 M H_2SO_4 under galvanostatic conditions at a current density of 200 mA cm^{-2}, with degradation times of 5, 10 and 20 min. During degradation, the solution was thoroughly stirred using a stirrer driven by a motor mounted on the dual-function cell via the grooves shown in Scheme 1(B). Each experiment was conducted in triplicate. Degradation was monitored using the same UHPLC system and chromatographic conditions as those described for the pharmaceutical capsule analysis in Section 2.5. The residual fraction of VF or DVF after each degradation period was calculated as the ratio of the analyte peak area in the degraded solution to that of the corresponding 1 mM standard solution, multiplied by 100 %.

3. Results and discussion

3.1. Effect of BDD_{GS} and BDD_{NS} surfaces and their termination

A free-standing BDD electrode featuring both the growth side (BDD_{GS}) and the nucleation side (BDD_{NS}) was employed to investigate surface-dependent electrochemical behaviour. These two surfaces exhibit distinct morphological and structural properties [28–30]. The BDD_{GS} is characterized by larger diamond (sp^3-hybridized carbon) grains, typically ranging from 4 to 54 μm in diameter, resulting in a lower density of grain boundaries where non-diamond (often sp^2-hybridized) carbon is commonly found. In contrast, the BDD_{NS} comprises smaller diamond grains (1–10 μm in diameter) and a higher density of grain boundaries and sp^2 carbon content. These intrinsic differences in morphology and composition are known to influence electrochemical performance, as previously demonstrated in our studies on glucose sensing [28] and carbamazepine degradation [30]. Therefore, we first examined how these two surfaces affect the electrochemical response toward VF and DVF.

Both BDD_{GS} and BDD_{NS} surfaces were subjected to electrochemical pre-treatments to induce either oxidized (O-) or hydrogenated (H-) terminations, as surface termination is a well-established factor governing the electrochemical properties of BDD electrodes [25,26]. Changes in surface termination were evaluated using cyclic voltammetry with the inner-sphere redox probe $[Fe(CN)_6]^{3-/4-}$, which is sensitive to surface oxygen functionalities introduced by anodic pre-treatment [26,51]. These modifications manifest as an increase in the peak-to-peak separation (ΔE_p). Conversely, cathodic pre-treatment, which reintroduces hydrogen termination, results in a decrease in ΔE_p. The corresponding voltammograms illustrating the behaviour of $[Fe(CN)_6]^{3-/4-}$ on differently terminated BDD surfaces are shown in Fig. S1 and display an increase in ΔE_p on oxidized O-BDD_{NS} and O-BDD_{GS} surfaces.

Cyclic voltammograms of VF and DVF (both 100.0 μM) were recorded on both oxidized and hydrogenated BDD_{GS} and BDD_{NS} surfaces in three different supporting electrolytes: 0.1 M H_2SO_4 (pH 0.7), 0.1 M PBS (pH 7.4), and 0.1 M NaOH (pH 13.0), using the respective potential windows available in each medium. The voltammograms obtained on BDD_{NS} are presented in Fig. 1, while those recorded on BDD_{GS} are shown in Fig. S2.

As clearly illustrated in Fig. 1, the most well-defined voltammetric responses for both VF and DVF on the BDD_{NS} surface were obtained in acidic medium (0.1 M H_2SO_4). Under these conditions, VF exhibited three well-resolved oxidation peaks on oxidized BDD_{NS} surface at +1.30 V, +1.45 V and +1.75 V. In contrast, DVF produced only a single peak at +1.34 V, indicating significant differences in the electrochemical behaviour of these compounds despite structural similarity (see the insets in Fig. 1(Aiii) and (Biii)). VF oxidized at slightly lower potentials on the oxidized surface, with higher peak intensities and improved definition, suggesting a preference for O-terminated BDD_{NS}. This preference for O-termination is consistent with previous work, where anodically oxidized O-BDD electrode yielded higher oxidation peak intensities and shifted oxidation processes to lower potentials compared with cathodically hydrogenated H-BDD surfaces [35].

Conversely, DVF exhibited a more pronounced response on H-terminated BDD_{NS}, indicating that hydrogen termination is more favourable for its detection. Thus, VF and DVF differ not only in the number of redox processes observed, but also in their preferred BDD_{NS} surface termination for optimal signal development. This behaviour can be assigned to their molecular structures: DVF contains a phenolic moiety, whereas VF bears a methoxy-substituted aromatic ring, leading to different oxidation mechanisms as discussed in detail in Section 3.2. Phenolic compounds (–OH directly attached to the aromatic ring), including bisphenol A, chlorophenols, butylated hydroxyanisole, and butylated hydroxytoluene, have been reported to yield better developed and often significantly more intense signals on H-terminated BDD compared to oxidized BDD [52–54].

In neutral medium (0.1 M PBS, pH 7.4), a notable decline in signal quality was observed. VF generated only a single, poorly defined peak, and only on O-BDD_{NS}. DVF continued to produce a single peak on both surface terminations, although the response was weaker and less well-defined than in acidic conditions. In alkaline medium (0.1 M NaOH, pH 13.0), neither VF nor DVF produced any detectable signals on BDD_{NS}, regardless of surface termination.

A markedly different behaviour was observed on the BDD_{GS} surface (Fig. S2). In acidic medium, VF yielded two poorly defined peaks, and only a faint signal was observed in PBS on O-BDD_{GS}. No signals were recorded for VF on H-BDD_{GS}, nor under alkaline conditions for either termination. DVF exhibited even poorer performance, with no discernible peaks on either O-BDD_{GS} or H-BDD_{GS} in any of the tested media, making it essentially undetectable on the BDD_{GS} surface.

Overall, the BDD_{NS} surface exhibited superior electrochemical performance toward both VF and DVF compared to BDD_{GS}. This behaviour

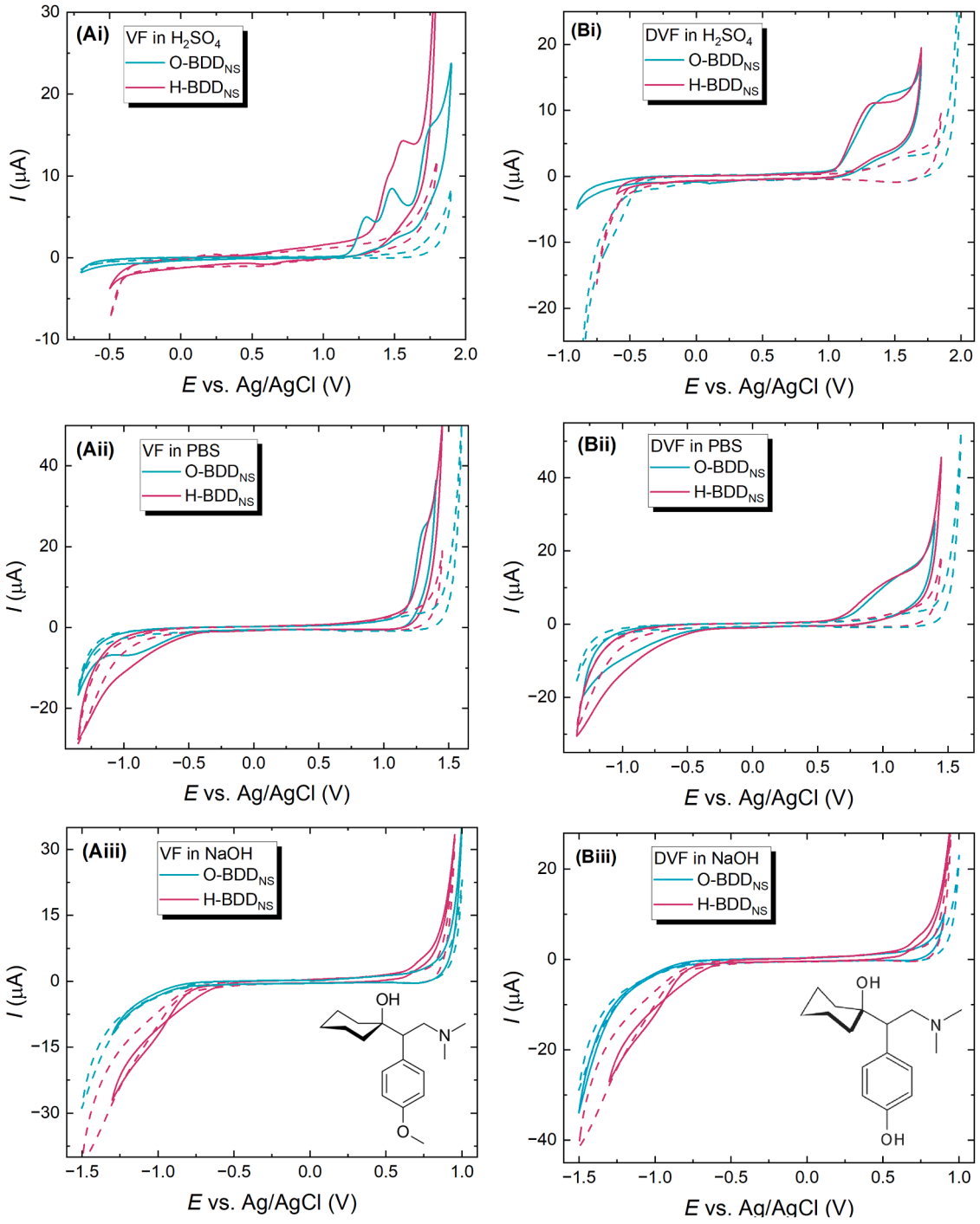

Fig. 1. Cyclic voltammograms of **(A)** 100.0 μM VF and **(B)** 100.0 μM DVF recorded on (green) oxidized and (pink) hydrogenated BDD_{NS} electrode surface in different supporting electrolytes: **(i)** 0.1 M H_2SO_4 (pH 0.7), **(ii)** 0.1 M PBS (pH 7.4), and **(iii)** 0.1 M NaOH (pH 13.0). The scan rate was 100 mV s^{-1}. Dashed lines represent the corresponding supporting electrolytes. The chemical structures of VF and DVF are shown as insets in (Aiii) and (Biii), respectively.

can be attributed to the smaller grain size and higher density of grain boundaries on the nucleation side, where sp^2-bonded carbon may reside [29]. Such sp^2-carbon domains are known to accelerate, or even enable, electron-transfer kinetics and facilitate redox processes; in our previous work with glucose, the strongest oxidation response was likewise obtained on BDD_{NS}, which contained the highest proportion of sp^2-bonded carbon among the tested BDD electrodes [28].

Consequently, all further voltammetric experiments were conducted using the BDD_{NS} electrode. Specifically, O-terminated BDD_{NS} was selected for VF due to its better-developed peaks, while H-terminated BDD_{NS} was used for DVF, where its signal was more pronounced.

3.2. *Effect of pH*

To further clarify the effect of pH, a thorough pH study was performed with both VF and DVF (both 100.0 μM) in BR buffers of pH 2.0–12.0 (with a step of pH 1.0), 0.1 M H_2SO_4 (pH 0.7) and 0.1 M NaOH (pH 13.0) on O-BDD_{NS} and H-BDD_{NS} electrodes, respectively. Obtained DPV curves are displayed in Fig. 2 (A, B) and show the strong dependence of both studied compounds on pH of the supporting electrolyte.

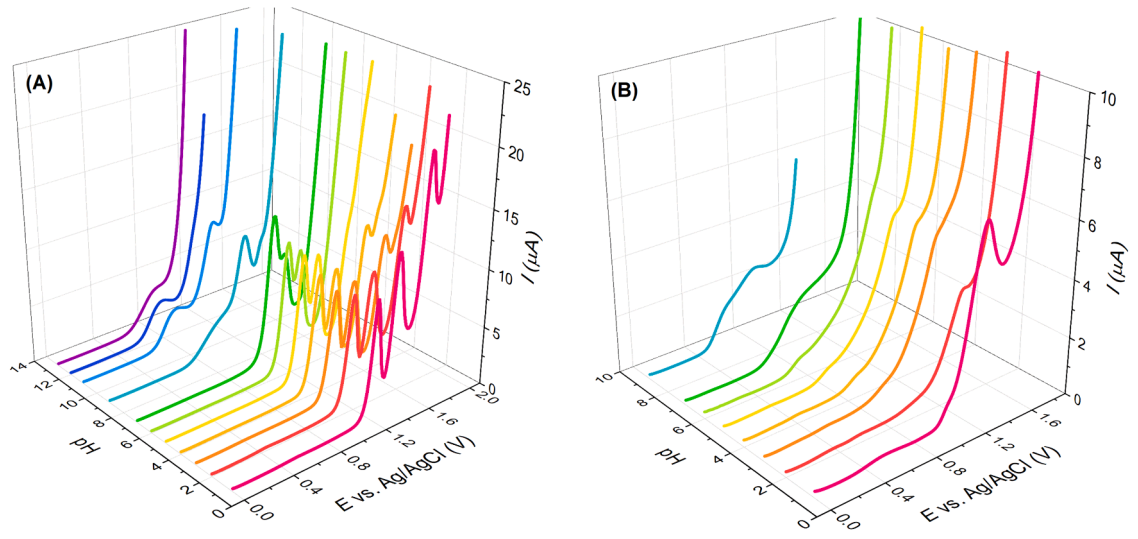

Fig. 2. DP voltammograms of **(A)** 100.0 μM VF recorded on O-BDD$_{NS}$ and **(B)** 100.0 μM DVF recorded on H-BDD$_{NS}$ in solutions with pH values ranging from 0.7 to 13.0.

VF contains a tertiary amine group (see Fig. 1(Aiii)) with a pK_A of approximately 9.4, and therefore exists predominantly in its protonated (cationic) form in acidic and neutral media (up to about pH 8). As clearly depicted in Fig. 2(A), the best-developed voltammetric signals were obtained in strongly acidic conditions (0.1 M H_2SO_4; pH 0.7), where electrostatic attraction between protonated amine groups of VF and oxygen-containing surface functionalities on O-BDD$_{NS}$ bearing partially negative charge (-$C^{\delta+}$–$O^{\delta-}$) likely promotes adsorption and electron transfer, as also previously reported for nitrogen-based heterocyclic compounds [26]. Three oxidation peaks are clearly observed up to pH 4.0; with increasing pH, the anodic potential window narrows and only the first two peaks remain, gradually merging between pH 5.0 and 7.0. From pH 9.0 to 11.0, a single main peak is observed together with a new, smaller peak at lower potential, which may be associated with the coexistence of protonated and neutral VF species near the pK_A. At even higher pH, the signals become progressively weaker and are almost completely suppressed at pH 13, indicating unfavourable conditions for VF oxidation. In a previous study of VF on a different type of BDD (thin-film), no oxidation peaks were observed for VF at pH values above 8, and an acidic medium of pH 2.0 was selected as the most suitable [35].

DVF exhibits two ionization equilibria, with pK_A values of approximately 8.3–8.9 for the dimethylamino group and ~10.1 for the phenolic group. Analogously to VF, it exists predominantly in its protonated form (at the tertiary amine) up to about pH 7. Nevertheless, analytically useful voltammetric signals for DVF were only obtained on H-BDD$_{NS}$ in highly acidic medium (0.1 M H_2SO_4, pH 0.7), as shown in Fig. 2(B); in other media, only a weak and poorly defined peak was observed. For both VF and DVF, the best-developed signals were thus achieved in strongly acidic 0.1 M H_2SO_4, which was therefore selected as the supporting electrolyte for subsequent studies.

Thus far, VF has been more frequently studied electrochemically than DVF [17–20,55–58] (see Table S1). On sp^2-carbon-based electrodes such as bare glassy carbon, pyrolytic graphite [55] or screen-printed carbon electrode [58], VF typically provides a single broad oxidation peak in the potential range of +0.6 V – +0.8 V. In contrast, on O-BDD$_{NS}$ three distinct oxidation peaks are observed at +1.20, +1.38, and +1.62 V, i.e., the first peak is shifted by roughly 400–600 mV to more positive potentials. For DVF, only a few electrochemical studies are available, including two on potentiometric determination [59,60] and two on voltammetric determination; in one case a reduction (cathodic) process was monitored [17], and in only one study an oxidation signal was reported, using a Nafion–carbon nanotube modified glassy carbon electrode [18], where the oxidation peak appeared at approximately +0.7 V. On H-BDD$_{NS}$, however, DVF oxidizes at +1.28 V, again shifted by nearly 600 mV relative to sp^2-carbon electrodes.

Such anodic shifts on BDD compared to sp^2-carbon electrodes have previously been described for phenolic and anisole-type aromatic species [61,62] and are commonly attributed to the heterogeneous nature of BDD, with a lower density of electronic states and fewer charge carriers, which can decrease electron transfer rates and increase overpotentials for redox reactions. In such a regime, successive electrochemical/chemical steps can become kinetically separated and appear as distinct peaks rather than collapsing into a single multi-electron wave, as is typically observed on sp^2-carbon materials, where the process is interpreted as an overall oxidation without resolving sub-steps. The multi-peak behaviour observed for VF on BDD is therefore ascribed to the combination of BDD's distinct electronic structure and surface chemistry, which promotes the separation of individual electron transfer steps. A similar phenomenon has been reported for the plant-growth regulator 1-naphthaleneacetic acid, where two distinct oxidation peaks were observed at BDD [63], whereas only a single oxidation peak was obtained at glassy carbon or carbon paste electrodes [64,65].

Finally, the differences in oxidation mechanism between VF and DVF, despite their very close structural similarity, also contribute to the distinct voltammetric behaviour observed on BDD. DVF contains a phenolic group (–OH directly attached to the aromatic ring), which is most likely the primary electroactive site. Its oxidation on BDD can be presumably described by the established mechanism for phenols: an initial one-electron/one-proton step to form a phenoxy radical [66], followed by rapid chemical reactions such as further oxidation to quinone-type species or irreversible radical–radical coupling or reaction with a parent molecule (dimerization and eventual polymeric film formation) [67]. These follow-up processes are predominantly chemical and are not resolved as separate faradaic events, so DVF gives a single anodic peak. In contrast, VF carries a methoxy group (–OCH_3) on the aromatic ring, and literature proposes a multi-step, two-electron mechanism: (i) initial oxidation of the aryl ring to an aryl radical cation; (ii) nucleophilic attack of water with loss of the methoxy group, yielding a phenolic/aryl radical intermediate; and (iii) a second electron transfer leading to a more oxidized quinone-like species. On BDD, a further (third) electron-transfer step is plausibly associated with oxidation of the tertiary amine to an aminium/iminium species, as the nitrogen lone pair can also be oxidized. This assumption is supported by previous studies on tertiary-amine-containing drugs: for example,

benzoylecgonine, measured at a BDD electrode, exhibits an irreversible oxidation process with a maximum peak around +2.10 V in acidic medium, attributed to oxidation of the tertiary amine in the tropane group [68].

3.3. Analytical performance

3.3.1. Optimization of DPV parameters

Given the irreversible oxidation behaviour of VF and DVF on the BDD_{NS} electrode surface (see Fig. 1), DPV was selected as the preferred technique for developing sensitive, selective, and reliable detection protocols. To this end, key DPV parameters affecting both peak current (signal intensity) and peak potential (position and shape), specifically modulation amplitude (A), modulation time (t), and potential step (E_s), were systematically optimized.

The optimization was performed independently for VF and DVF (each at a concentration of 100.0 μM) using O-BDD_{NS} for VF and H-BDD_{NS} for DVF. The influence of each parameter was evaluated within the following ranges: A 10–150 mV (for VF) and 10–250 mV (for DVF), t 5–50 ms, and E_s 5–25 mV. During the optimization process, two parameters were held constant while the third was varied to assess its effect on the analytical response. Fig. S3 illustrates the dependence of the recorded peak currents of VF and DVF on the tested values of each DPV parameter. The final DPV conditions were selected as a compromise between maximizing peak intensity and maintaining well-defined peak shapes. The optimized parameters were: (i) VF at O-BDD_{NS}: A 115 mV, t 10 ms, E_s 15 mV; (ii) DVF at H-BDD_{NS}: A 200 mV, t 20 ms, E_s 15 mV. The DP voltammograms obtained using these optimized parameters are depicted in Fig. 3 and compared with those recorded using initially selected, non-optimized parameters.

3.3.2. Stability of DVF and VF voltammetric responses

A series of experiments was conducted under optimized conditions, i.e., BDD surface state, supporting electrolyte and DPV parameters, to evaluate the stability of the voltammetric signals of VF and DVF (both 100.0 μM). Ten consecutive DPV scans were performed under three different conditions: (i) without any stirring or electrode pre-treatment between scans, (ii) with stirring of the solution between scans, and (iii) with an electrochemical pre-treatment step applied between scans, i.e., 30 s of anodic oxidation for O-BDD_{NS} or 30 s of cathodic reduction for H-BDD_{NS}. Both the peak potentials and peak currents were monitored. While peak potentials remained essentially stable (with a maximum deviation of ±0.010 V), peak currents varied depending on the measurement conditions, as shown in Fig. 4 and Table S2.

In the first set of measurements, i.e., ten successive DPV scans without stirring or pre-treatment, a continuous decline in signal intensity was observed for both VF and DVF. This signal deterioration is attributed to two main factors: (1) a decrease in the local concentration of the analyte near the electrode surface, and (2) progressive fouling of the BDD_{NS} surface due to adsorption of oxidation products.

When the solution was stirred between measurements, the decrease in peak currents was significantly mitigated for VF, with reductions limited to 13–23 %. Stirring likely restores the analyte concentration at the electrode surface and partially removes adsorbed species. As illustrated in Fig. 4(A), although a decline in peak currents still occurred, it was substantially smaller than in the unstirred case (which showed a 60–77 % decrease). In contrast, DVF exhibited less improvement with stirring, and a 55 % decline in peak current was still observed after ten scans (Fig. 4(B)). This behaviour is consistent with the proposed oxidation mechanism: DVF oxidizes via a phenoxy-radical pathway, which can lead to the formation of dimeric and polymeric products that strongly adsorb on the H-BDD_{NS} surface and cause pronounced fouling, not prevented by simple stirring. For VF, the oxidation products are presumably less prone to form strongly adherent polymeric films, and any fouling appears weaker and more easily mitigated by stirring, which aligns with the different oxidation pathways and products discussed in detail in Section 3.2.

Notably, incorporation of the respective electrochemical pre-treatment step between scans ensured highly reproducible signals for both compounds. Excellent intra-day repeatability (n = 10) was achieved, with relative standard deviations (RSD) not exceeding 2.1 % (see Table S2). These results confirm the high stability and reliability of the VF and DVF signals when a simple, quick reactivation procedure is employed.

An additional advantage is that the BDD_{NS} electrode operates effectively in its unmodified form. If required, the surface can be conveniently reactivated by extending the pre-treatment step, eliminating the need for complex and time-consuming modification protocols typically required for sp^2-carbon-based electrodes [17–20,55–57,69]. Moreover, such modified electrodes often suffer from signal instability and fabrication reproducibility issues, making BDD_{NS} a robust and practical choice for reliable electrochemical detection of these antidepressants.

3.3.3. Concentration dependences

Next, the concentration dependence of both antidepressants was investigated under optimized conditions using the BDD_{NS} electrode. The resulting DP voltammograms are depicted in Fig. 5. Key analytical parameters, including linear range, sensitivity, as well as the calculated LOD and LOQ values are summarized in Table 1, while the calibration graphs for the individual VF peaks and DVF are depicted in Fig. S4.

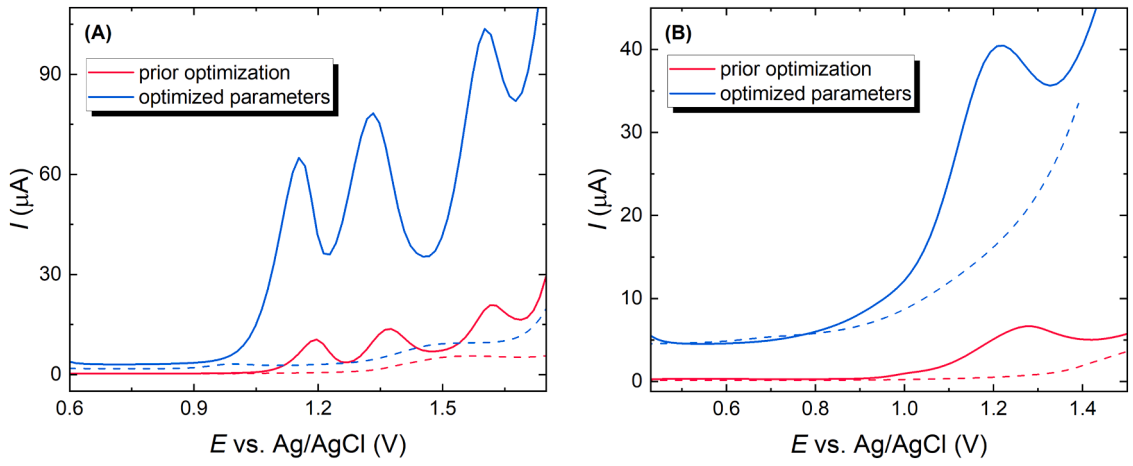

Fig. 3. DP voltammograms of **(A)** 100.0 μM VF recorded on O-BDD_{NS} and **(B)** 100.0 μM DVF recorded on H-BDD_{NS}, comparing signals obtained using initially selected (pre-optimization, pink line) and optimized (blue line) DPV parameters. Dashed line corresponds to the supporting electrolyte (0.1 M H_2SO_4).

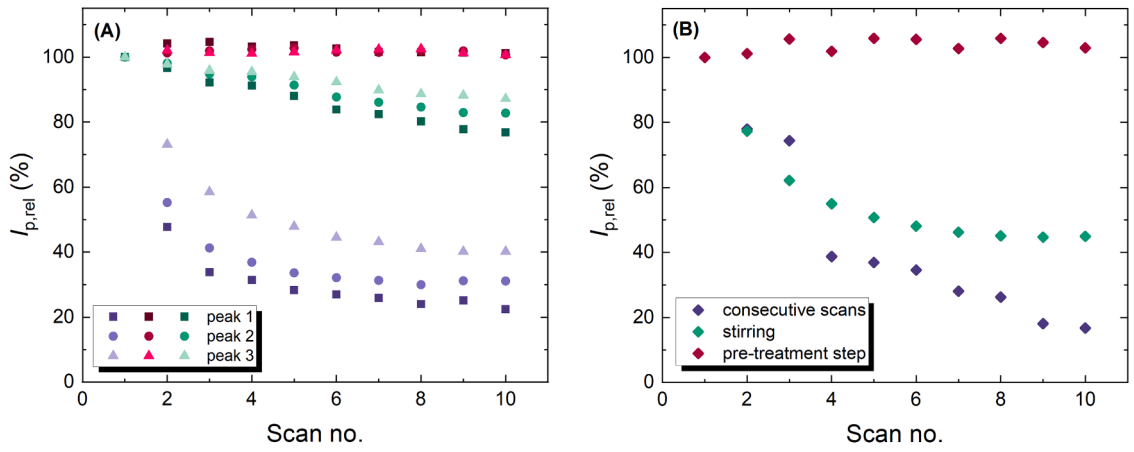

Fig. 4. Relative peak currents ($I_{p,rel}$) of **(A)** three oxidation peaks of 100.0 μM VF recorded on O-BDD$_{NS}$ and **(B)** a single peak of 100.0 μM DVF recorded on H-BDD$_{NS}$. Ten consecutive DPV scans were performed under three conditions: without any intervention between scans (purple symbols), with stirring of the solution between scans (green symbols), and with electrochemical surface reconditioning between scans – 30 s of anodic oxidation (+2.4 V) for O-BDD$_{NS}$ or 30 s of cathodic reduction (−2.4 V) for H-BDD$_{NS}$.

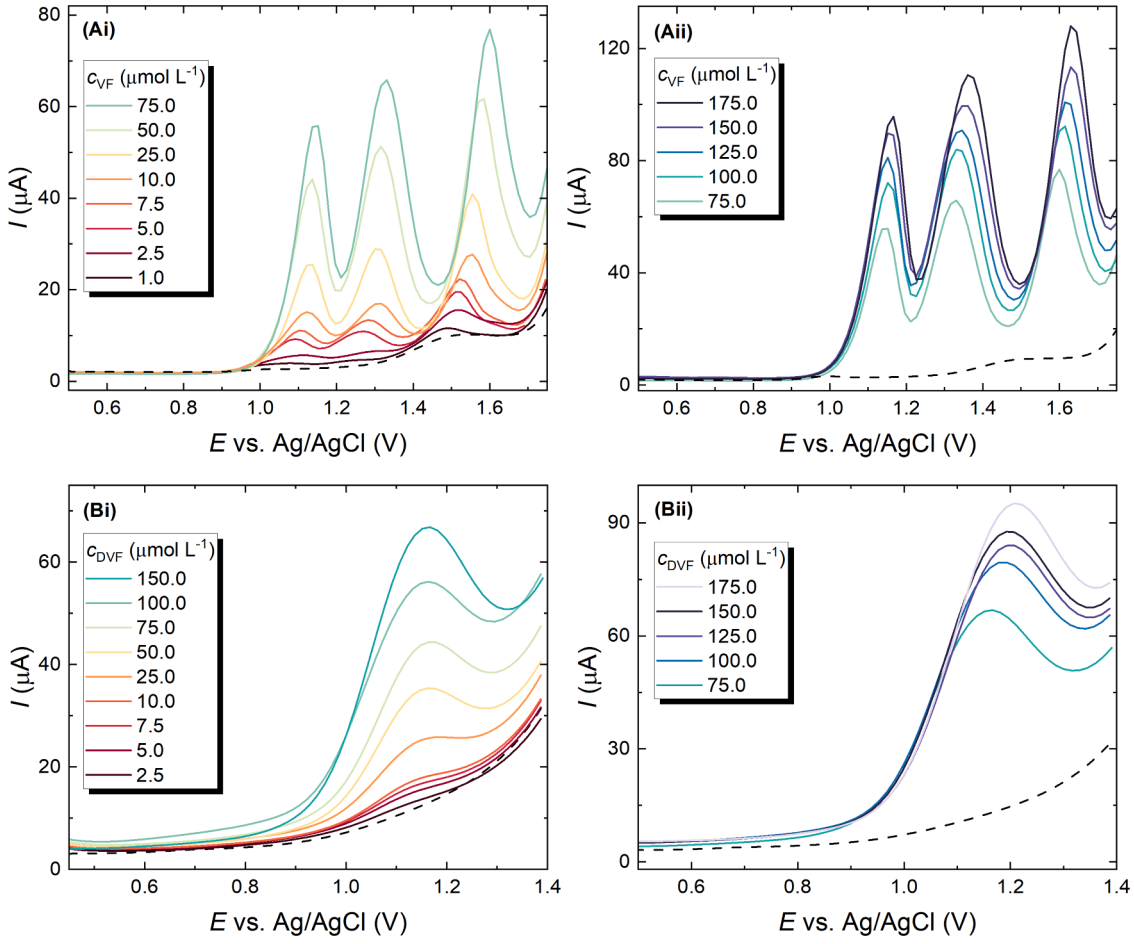

Fig. 5. DP voltammograms of **(A)** VF recorded on O-BDD$_{NS}$ and **(B)** DVF recorded on H-BDD$_{NS}$ at various concentration levels. Dashed lines correspond to the supporting electrolyte (0.1 M H_2SO_4).

Fig. 5 clearly shows that the oxidation peak currents of both VF and DVF increase with increasing concentration, and two linear ranges were obtained for each antidepressant. The LOQ values are either below or very close to 1.0 μM, which is relevant given that therapeutic plasma concentrations are approximately 0.5–2.2 μM for VF and 0.3–1.5 μM for DVF [70], with higher levels associated with an increased risk of toxicity. In environmental waters, however, VF and DVF typically occur at concentrations several orders of magnitude lower (nM range) [8], and the developed voltammetric methods cannot be applied directly to untreated samples; an appropriate preconcentration step (e.g., extraction) would be required. When compared with previously reported electroanalytical methods (summarized in Table S1), the analytical figures of

Table 1
Analytical parameters of VF and DVF concentration dependences recorded by developed DPV methods.

Compound	Linear range (μM)	Intercept (μA)	Slope (μA μM^{-1})	*R*	LOD (μM)	LOQ (μM)
O-BDD$_{NS}$						
VF – peak 1	1.0 – 75.0	0.49 ± 0.52	0.547 ± 0.017	0.9962	0.35	1.15
	75.0 – 175.0	19.2 ± 0.07	0.278 ± 0.005	0.9995		
VF – peak 2	1.0 – 75.0	0.48 ± 0.54	0.625 ± 0.018	0.9969	0.29	0.89
	75.0 – 150.0	27.6 ± 1.0	0.236 ± 0.008	0.9988		
VF – peak 3	1.0 – 50.0	4.93 ± 0.91	0.726 ± 0.044	0.9876	0.14	0.42
	50.0 – 175.0	26.1 ± 2.0	0.287 ± 0.017	0.9931		
H-BDD$_{NS}$						
DVF	2.5 – 150.0	−0.06 ± 0.29	0.226 ± 0.004	0.9988	0.34	1.04
	150.0 – 275.0	20.5 ± 0.6	0.086 ± 0.002	0.9987		

merit obtained here are comparable, and in some cases superior, while using a robust, unmodified BDD electrode and thus avoiding complex and time-consuming surface modification procedures.

3.3.4. *Simultaneous detection of VF and DVF*

DVF is the main active metabolite of VF, and both compounds thus co-occur in biological matrices (e.g., blood, urine) as well as in environmental waters. It is therefore important to assess whether VF and DVF can be reliably determined in the presence of each other using the proposed DPV methods. A notable advantage of the developed approach is that VF and DVF exhibit different preferences toward BDD surface termination (VF on O-BDD$_{NS}$, DVF on H-BDD$_{NS}$), which can be exploited to improve signal discrimination in mixtures. The simultaneous detection was evaluated in the lower micromolar concentration ranges, which are more relevant for physiological levels and for environmental samples (the latter after an appropriate preconcentration step). The corresponding analytical parameters, derived from the DP voltammograms shown in Fig. 6, are summarized in Table S3.

Three calibration strategies were investigated. In the first, a dual-variation calibration (Fig. 6(A)), the concentrations of both VF and DVF were simultaneously increased stepwise from 1.0 to 10.0 μM on O-BDD$_{NS}$. Under these conditions, the second and third oxidation peaks of VF remained well resolved and could be reliably quantified, whereas the DVF peak partially overlapped with the first VF peak but could still be evaluated separately. In the second strategy (Fig. 6(B)), the DVF concentration was fixed at 5.0 μM and the VF concentration was varied (from 1.0 to 14.0 μM) on O-BDD$_{NS}$. Again, the second and third VF peaks were essentially unaffected by DVF and could be determined with very good selectivity. The first VF peak was influenced by the presence of DVF at low VF levels but became well defined and suitable for evaluation at VF concentrations ≥ 4.0 μM. In the third strategy (Fig. 6(C)), the VF concentration was held constant at 10.0 μM while the DVF concentration was varied (from 4.0 to 20.0 μM) on H-BDD$_{NS}$. The main DVF peak could be clearly discerned and quantified, although a small contribution from the first VF peak appeared at higher potential values. Overall, these results demonstrate that, by exploiting the distinct surface-termination preferences and the multi-peak behaviour of VF, simultaneous determination of VF and DVF is feasible within the investigated concentration ranges.

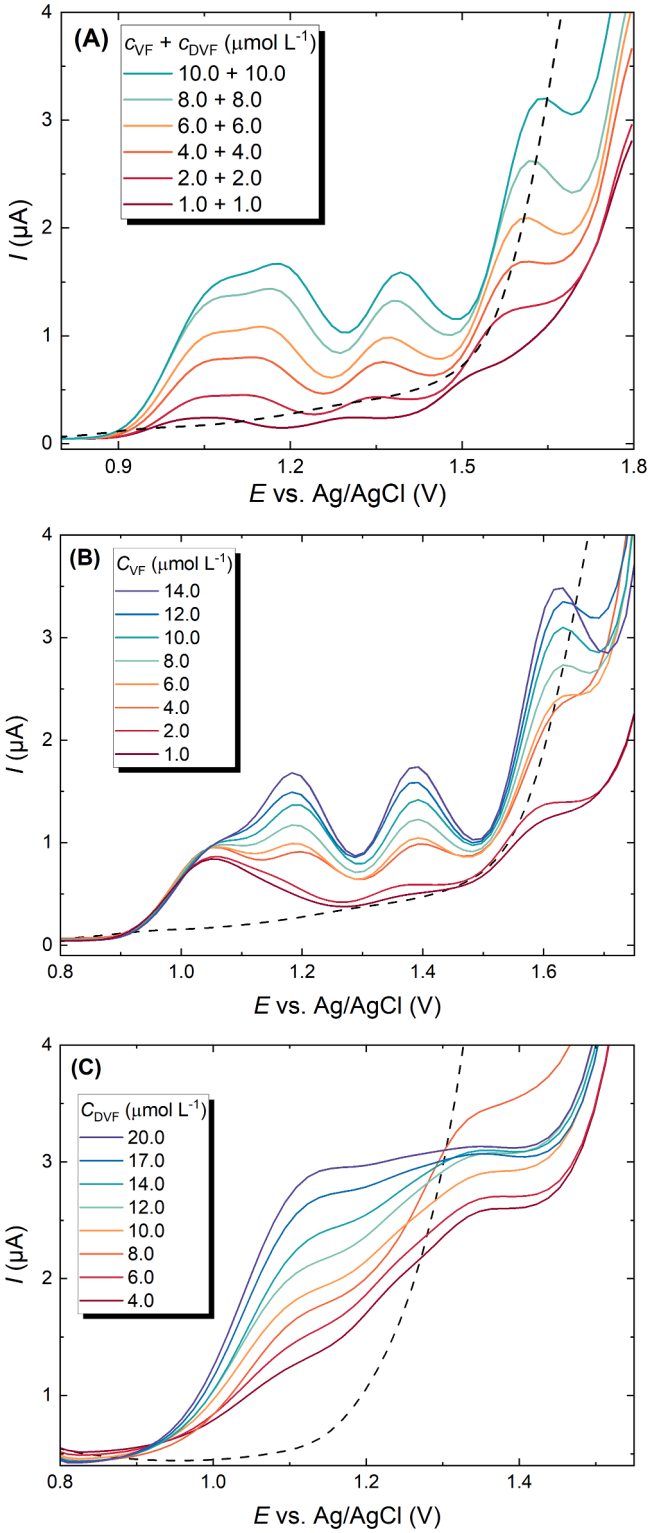

Fig. 6. DP voltammograms recorded under the following conditions: **(A)** simultaneous variation of VF and DVF concentrations (dual-variation calibration) on O-BDD$_{NS}$, **(B)** DVF kept constant at 5.0 μM while VF concentration was varied, recorded on O-BDD$_{NS}$, **(C)** VF kept constant at 10.0 μM while DVF concentration was varied, recorded on H-BDD$_{NS}$. Dashed lines represent the background response of the supporting electrolyte (0.1 M H_2SO_4).

3.4. *Interference study*

The selectivity of the proposed DPV methods for VF and DVF

detection was further evaluated by examining the voltammetric response of 10.0 μM solutions of each analyte in the presence of common interfering compounds at varying concentrations. Representative DP voltammograms recorded in the presence of interferents are shown in Fig. S5, while Fig. 7 summarizes the extent to which VF and DVF peak currents were affected by each interferent.

Both VF (all three peaks) and DVF showed minimal interference from a 500-fold excess of carbohydrates (glucose and sucrose) and from citric acid at concentrations up to 1000 μM. However, interference became more pronounced with electroactive compounds such as ascorbic acid and dopamine. Ascorbic acid (vitamin C), which is typically present in blood at concentrations between 10 and 115 μM [71], had limited impact on VF peaks 1 and 3 and the DVF signal at physiological levels. However, VF peak 2 was significantly affected at ascorbic acid concentrations from and above 100 μM, and DVF signal intensity deviated beyond the ±10 % tolerance threshold at 500 μM, a concentration not expected in real biological samples.

Dopamine, present in plasma at low concentrations (≤ 0.1 μM), did not interfere with VF detection even at elevated levels (250 μM for peaks 1 and 2, and 100 μM for peak 3). In contrast, dopamine had a more pronounced effect on DVF detection, suggesting potential challenges in selective quantification of DVF in dopamine-rich environments.

3.5. Real sample analysis

Finally, the suitability of the proposed DPV methods for practical applications was verified by analysing environmental river water (VF and DVF) and pharmaceutical capsules (VF) using the standard addition method. The determined concentrations and corresponding recoveries are summarized in Table 2 for river water and Table 3 for pharmaceutical capsules.

For VF in river water, the sample was diluted with 0.1 M H_2SO_4 and measured on O-BDD_{NS} (Fig. 8(A)). A small background peak was observed around +1.5 V in the unspiked sample. After spiking with 5.0 μM VF, the third VF peak was partially affected by this background response; however, the first two VF peaks remained well defined and were used for quantification by standard addition, yielding recoveries of 106.4 % and 94.4 % for the first and second VF peak, respectively. For DVF, recorded on H-BDD_{NS} (Fig. S6), no interfering peak from the diluted river water was observed in the potential region of interest, and the DVF peak was clearly distinguishable after spiking, enabling reliable quantification by the standard addition method.

The capsule extracts were analysed by both DPV and UHPLC-UV methods. Using DPV (Fig. 8(B)), VF contents determined from peak 1 and peak 2 were 152.7 ± 7.5 mg (101.8 % recovery) and 154.6 ± 5.6 mg (103.1 % recovery), respectively. These values are in good agreement with the label claim (150 mg) and with the UHPLC-UV reference method (150.0 ± 5.3 mg; 100 % recovery), confirming the accuracy of the DPV

Table 2
Determination of VF and DVF in spiked river water samples by DPV methods, using the standard addition method ($n = 3$).

Compound	Spiked (μM)	Found (μM) ± SD	Recovery (%)[a]	RSD (%)
VF peak 1	5.0	5.32 ± 0.40	106.4	8.0
VF peak 2	5.0	4.72 ± 0.37	94.4	7.4
DVF	5.0	5.49 ± 0.55	109.8	11.0

[a] Recovery (%) = (found concentration / spiked concentration) × 100.

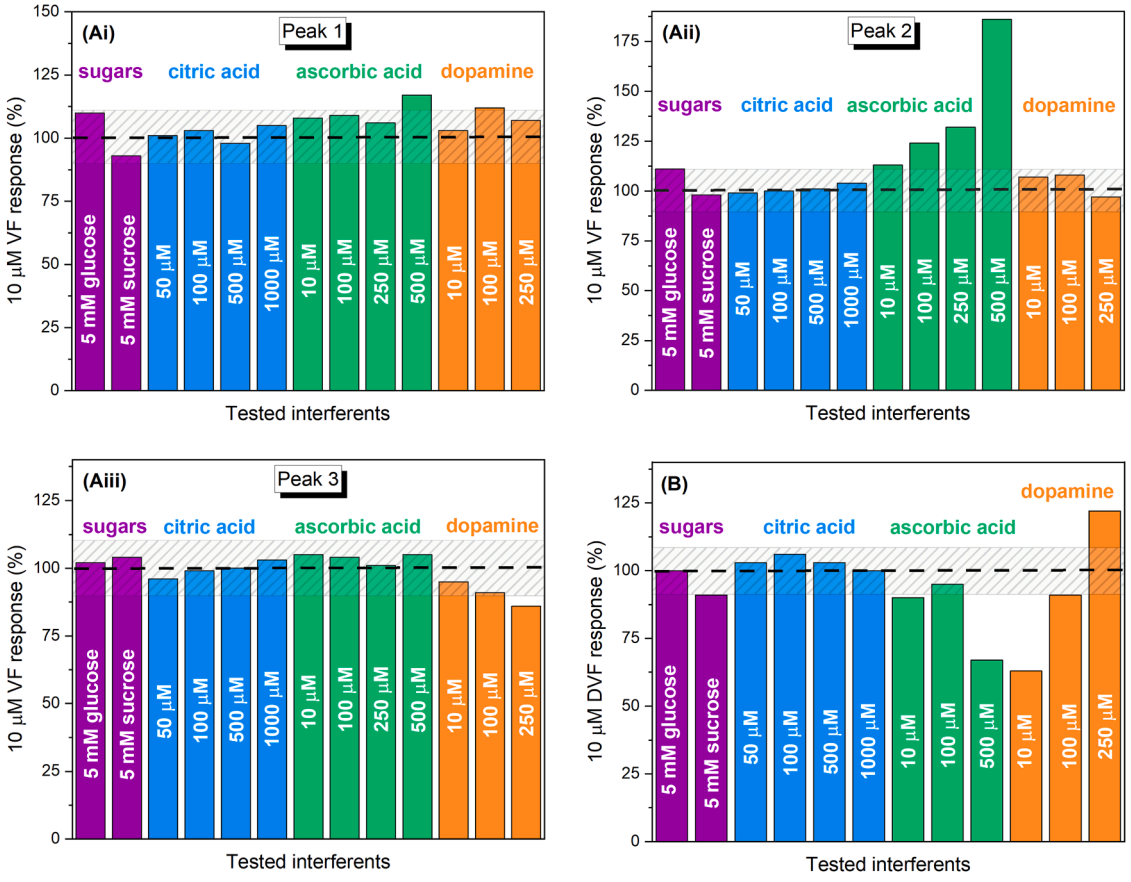

Fig. 7. Relative DP voltammetric responses of **(A)** 10.0 μM VF for each of its three peaks **(i-iii)** recorded on the O-BDD_{NS} electrode and **(B)** 10.0 μM DVF recorded on the H-BDD_{NS} electrode, in the presence of various interfering compounds at different concentration levels. Measurements were conducted in 0.1 M H_2SO_4. The dashed grey zones represent the acceptable ±10 % variation in peak current intensity, indicating the tolerance range for signal interference.

Table 3
Determination of VF in pharmaceutical capsules by DPV (on O-BDD_{NS}) and UHPLC-UV, using the standard addition method ($n = 3$).

Method	Label claim (mg/ capsule)	Found (mg/capsule) ± SD	Recovery (%)[a]	RSD (%)
DPV – VF peak 1	150	152.7 ± 7.5	101.8	5.0
DPV – VF peak 2	150	154.6 ± 5.6	103.1	3.7
UHPLC-UV	150	150.0 ± 5.3	100.0	3.5

[a] Recovery (%) = (found mg VF in capsule / labelled VF content in capsule) × 100.

approach for routine quality control. Overall, recoveries were close to 100 % and the RSD values were at or below 5 %, indicating good precision of both methods.

3.6. *Degradation kinetics and proof-of-concept validation in the 3D-printed dual-function cell*

Since BDD_{NS} proved more suitable for electroanalytical measurements, the opposite face, BDD_{GS}, was selected as the anode for degradation experiments, in line with our previous work demonstrating its good performance in electrochemical pollutant removal [30].

Degradation experiments were carried out to evaluate the performance of the 3D-printed dual-function cell in terms of VF and DVF removal efficiency, kinetics, repeatability, and its ability to couple degradation with in situ detection. Solutions of 1.0 mM VF or DVF in 0.1 M H_2SO_4 were subjected to galvanostatic electrolysis on strongly oxidized O-BDD_{GS} at a current density of 200 mA cm^{-2} (the cell voltage fluctuated between +17 V and +23 V). In this medium, the generation of hydroxyl radicals and sulphate radical anions is expected, both of which are strong oxidants capable of efficiently degrading organic pollutants [30,72]. Such a high current density can be applied because of the free-standing nature of the BDD electrode, which avoids the stability, adhesion and delamination issues often encountered with BDD thin films grown on metal substrates. For thin-film BDD electrodes, current densities are typically limited to about 50–100 mA cm^{-2} to prevent film damage. In contrast, in a recent study [73], a free-standing BDD electrode was employed for the electrochemical degradation of perfluorobutanoic and perfluorobutanesulfonic acids in a 3D-printed recirculating flow cell, and current densities of ≥ 390 mA cm^{-2} were sustained for several hours without any obvious signs of electrode corrosion. This furthers confirm the robustness of free-standing BDD under demanding EAOP conditions.

The relative concentrations of VF and DVF were monitored by UHPLC-UV as a function of degradation time to determine degradation kinetics and reproducibility. As shown in Fig. 9(A), the decay of both VF and DVF followed an exponential trend consistent with first-order behaviour. Owing to the large excess of electrogenerated hydroxyl radicals over antidepressant molecules, the degradation process was actually treated as pseudo-first-order, in line with previous reports for anodic oxidation on non-active anodes [74,75]. The apparent degradation rate constants obtained were $k_{app,VF} = 0.10\ min^{-1}$ for VF and $k_{app,DVF} = 0.17\ min^{-1}$ for DVF. After 20 min of treatment, approximately 97 % of each antidepressant was removed, and no additional chromatographic peaks attributable to degradation products were detected. Error bars, representing 95 % confidence intervals from triplicate experiments, were within 9 % of the relative amount values, indicating satisfactory repeatability and confirming O-BDD_{GS} as a suitable electrode material for efficient removal of these pollutants in the proposed cell configuration.

To demonstrate the dual degradation-detection functionality of the device, a proof-of-concept in situ monitoring was performed by DPV for VF. With the electrode orientation described in Section 2.6, DP voltammograms of an initially 1.0 mM VF solution in 0.1 M H_2SO_4 were recorded on O-BDD_{NS} after 0, 3, 6, and 15 min of degradation (Fig. 9(B)). After 3 and 6 min, the first and second VF peaks decreased markedly, whereas the third peak increased substantially after 3 min and then decreased at 6 min, however, remaining higher than in the undegraded solution. This behaviour suggests the transient formation of an electroactive intermediate generated during VF degradation, contributing to the third peak. After 15 min of electrolysis, no peaks corresponding to VF were observed on O-BDD_{NS}, in agreement with the UHPLC-UV results. These findings not only validate the proof-of-concept operation of the 3D-printed cell but also highlight its methodological novelty: within a single free-standing BDD/3D-printed platform, efficient electrochemical degradation on one BDD face is coupled with real-time voltammetric monitoring on the opposite side, reducing reliance on external analytical instrumentation such as HPLC.

Using VF and DVF as model antidepressants, the current scope of our dual-function platform can be outlined as follows: The approach is well suited for applications where analyte levels are in the low–mid micromolar range (e.g., pharmaceutical formulations, spiked laboratory samples or enriched environmental matrices) and where acidification to 0.1 M H_2SO_4 is acceptable. At the same time, the requirement for strongly acidic medium and the present LOD values mean that direct monitoring of trace-level (sub-nanomolar) environmental

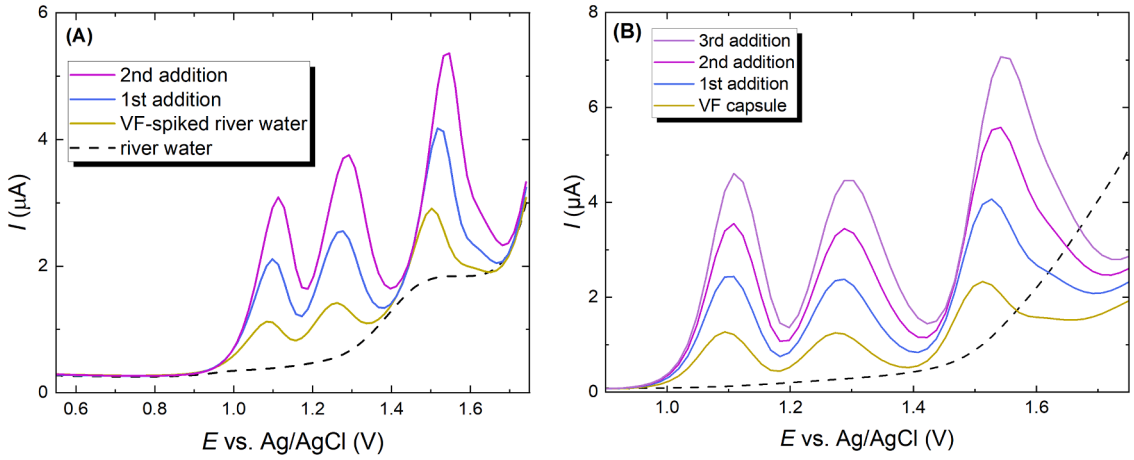

Fig. 8. **(A)** DP voltammograms recorded in the river water sample diluted with 0.1 M H_2SO_4 (1:9) and spiked with 5.0 μM VF, followed by the two standard additions (both 100 μL, 1 mM VF) on O-BDD_{NS}. Dashed line corresponds to the diluted river water without spiked VF. **(B)** DP voltammograms recorded in the pharmaceutical capsule solution (10.0 μM VF), followed by three standard additions (each 100 μL, 1 mM VF) on O-BDD_{NS}. Dashed line corresponds to 0.1 M H_2SO_4.

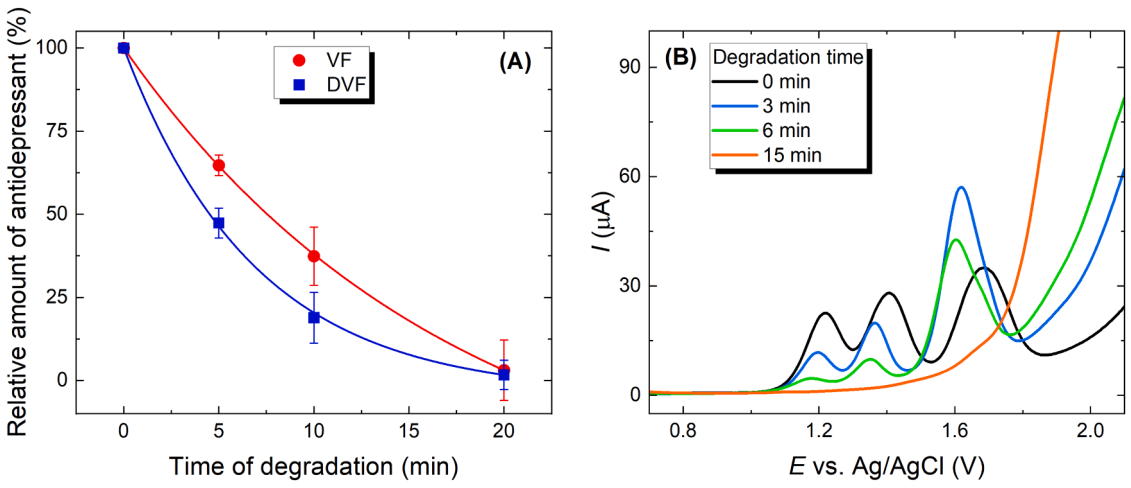

Fig. 9. **(A)** Dependence of the relative amount of (red circle) VF and (blue square) DVF on degradation time for their 1.0 mM solutions subjected to electrochemical degradation on O-BDD_{GS} (at 200 mA cm^{-2}). Error bars represent 95 % confidence intervals based on triplicate measurements. **(B)** DP voltammograms recorded on O-BDD_{NS} after (■) 0, (■) 3, (■) 6, and (■) 15 min of degradation of 1 mM VF under galvanostatic conditions.

concentrations would still require an appropriate preconcentration step. The present design operates in batch mode with a small volume (12 mL); such conditions are appropriate for proof-of-concept kinetic and mechanistic studies, but long-term material stability and operation under realistic pollutant levels and continuous solution flow remain subjects for future work.

On the other hand, herein presented 3D-printed dual-function cell is small and compact, and in combination with modern miniaturized potentiostats it is well suited for mobile, rapid field monitoring. Stereolithography-based 3D printing, as used here, is widely accessible, cost-effective and highly suitable for rapid prototyping and custom geometries, while the free-standing BDD electrode offers the clear advantage of sustaining substantially higher current densities than BDD thin films on metallic supports. In addition, proposed "detect-and-degrade" methodology can, in principle, be extended to other organic pollutants present in a variety of environmental matrices. For detection purposes, the selected side of the free-standing BDD could be further tailored, for example by controlled introduction of sp^2-carbon domains via laser micromachining [76,77], to fine-tune sensitivity and selectivity.

4. Conclusion

This study presents a comprehensive electrochemical strategy for the detection and degradation of the antidepressants VF and DVF using a single free-standing BDD electrode integrated into a 3D-printed dual-function cell. By comparing the nucleation (BDD_{NS}) and growth (BDD_{GS}) faces under controlled surface terminations, BDD_{NS} was identified as the superior surface for electroanalytical applications, whereas BDD_{GS} was then selected for electrochemical advanced oxidation.

On O-BDD_{NS}, VF exhibited three well-resolved oxidation peaks, in contrast to the single peak typically reported on sp^2-carbon electrodes, while DVF yielded a single peak on H-BDD_{NS}. This behaviour reflects both the differing oxidation mechanisms of VF and DVF and the ability of BDD to kinetically separate successive electron transfer steps. Optimized DPV protocols allowed for low micromolar limits of detection (down to 0.35 μM for first VF peak and 0.34 μM for DVF), broad linear ranges, and excellent signal stability when combined with brief electrochemical reconditioning steps.

The developed DPV methods displayed good tolerance toward common interferents and enabled simultaneous determination of VF and DVF by exploiting their distinct surface-termination preferences and the multi-peak response of VF. Practical applicability was demonstrated through analyses of river water and commercial capsules, where recoveries were generally close to 100 %, confirming the robustness of the unmodified BDD_{NS} surface for real-sample measurements.

In the custom 3D-printed cell, electrochemical degradation of 1.0 mM VF and DVF on BDD_{GS} in 0.1 M H_2SO_4 achieved approximately 97 % removal within 20 min, following pseudo-first-order kinetics. In situ DPV on O-BDD_{NS} allowed real-time tracking of VF decay and its oxidation products, demonstrating the feasibility of coupling degradation and electrochemical monitoring in a single, compact platform.

Overall, this work illustrates how free-standing BDD materials and additive manufacturing can be synergistically combined to create multifunctional electrochemical systems capable of both sensitive detection and efficient removal of pharmaceutical contaminants, offering a promising route toward integrated monitoring–remediation technologies for water quality management.

CRediT authorship contribution statement

Martin Šefčík: Writing – original draft, Visualization, Methodology, Investigation, Funding acquisition, Formal analysis, Data curation. **Ghazaleh Kholafazadehastamal:** Writing – original draft, Visualization, Methodology, Investigation, Formal analysis, Data curation. **Thomas Peeters:** Investigation, Formal analysis, Data curation. **Jan Fischer:** Writing – review & editing, Visualization, Supervision, Methodology. **Anna Kubíčková:** Writing – review & editing, Supervision, Methodology. **Clive E. Hall:** Writing – review & editing, Resources. **Josephus G. Buijnsters:** Writing – review & editing, Supervision, Conceptualization. **Simona Baluchová:** Writing – review & editing, Writing – original draft, Visualization, Supervision, Project administration, Funding acquisition, Formal analysis, Data curation, Conceptualization.

Declaration of competing interest

The authors declare that they have no known competing financial interests or personal relationships that could have appeared to influence the work reported in this paper.

Acknowledgements

The research was carried out within the framework of Specific University Research (SVV 260793). S.B. gratefully acknowledges the support of the Charles University Primus program (grant no. PRIMUS/25/SCI/020). M. Š. is thankful for financial support provided by the Grant Agency of Charles University (project no. 392825). The authors are

thankful to Mintres B.V. (the Netherlands) for providing the free-standing, polycrystalline BDD electrode.

Supplementary materials

Supplementary material associated with this article can be found, in the online version, at doi:10.1016/j.electacta.2026.148353.

Data availability

Data will be made available on request.

References

[1] Q. Liu, H. He, J. Yang, X. Feng, F. Zhao, J. Lyu, Changes in the global burden of depression from 1990 to 2017: findings from the global burden of disease study, J. Psychiatr. Res. 126 (2020) 134–140, https://doi.org/10.1016/j.jpsychires.2019.08.002.

[2] C. Saka, Ö. Şahin, Determination of serotonin-norepinephrine reuptake inhibitor antidepressants in pharmaceuticals and biological material, Crit. Rev. Anal. Chem. 43 (1) (2013) 2–34, https://doi.org/10.1080/10408347.2011.645377.

[3] Drugbank. *Venlafaxine*. https://go.drugbank.com/drugs/DB00285 (accessed 15-10-2025).

[4] Drugbank. *Desvenlafaxine*. https://go.drugbank.com/drugs/DB06700 (accessed 15-10-2025).

[5] Y. Ouarda, F. Bouchard, A. Azaïs, M.-A. Vaudreuil, P. Drogui, R. Dayal Tyagi, S. Sauvé, G. Buelna, R. Dubé, Electrochemical treatment of real hospital wastewaters and monitoring of pharmaceutical residues by using surrogate models, J. Environ. Chem. Eng. 7 (5) (2019) 103332, https://doi.org/10.1016/j.jece.2019.103332.

[6] J.R. Dominguez, T. González, S.E. Correia, M.M. Núñez, Emerging contaminants decontamination of WWTP effluents by BDD anodic oxidation: a way towards its regeneration, Water. (Basel) 15 (9) (2023), https://doi.org/10.3390/w15091668.

[7] P.C. Rúa-Gómez, W. Püttmann, Degradation of lidocaine, tramadol, venlafaxine and the metabolites O-desmethyltramadol and O-desmethylvenlafaxine in surface waters, Chemosphere 90 (6) (2013) 1952–1959, https://doi.org/10.1016/j.chemosphere.2012.10.039.

[8] J.L. Wilkinson, A.B.A. Boxall, D.W. Kolpin, K.M.Y. Leung, R.W.S. Lai, C. Galbán-Malagón, A.D. Adell, J. Mondon, M. Metian, R.A. Marchant, et al., Pharmaceutical pollution of the world's rivers, Proc. Natl. Acad. Sci. U.S.A. 119 (8) (2022) e2113947119, https://doi.org/10.1073/pnas.2113947119.

[9] P. Sehonova, Z. Svobodova, P. Dolezelova, P. Vosmerova, C. Faggio, Effects of waterborne antidepressants on non-target animals living in the aquatic environment: a review, Sci. Total Environ. 631-632 (2018) 789–794, https://doi.org/10.1016/j.scitotenv.2018.03.076.

[10] A. Salahinejad, A. Attaran, D. Meuthen, D.P. Chivers, S. Niyogi, Proximate causes and ultimate effects of common antidepressants, fluoxetine and venlafaxine, on fish behavior, Sci. Total Environ. 807 (2022) 150846, https://doi.org/10.1016/j.scitotenv.2021.150846.

[11] S. Fekadu, E. Alemayehu, R. Dewil, B. Van der Bruggen, Pharmaceuticals in freshwater aquatic environments: a comparison of the African and European challenge, Sci. Total Environ. 654 (2019) 324–337, https://doi.org/10.1016/j.scitotenv.2018.11.072.

[12] M. Čelić, A. Jaén-Gil, S. Briceño-Guevara, S. Rodríguez-Mozaz, M. Gros, M. Petrović, Extended suspect screening to identify contaminants of emerging concern in riverine and coastal ecosystems and assessment of environmental risks, J. Hazard. Mater. 404 (2021) 124102, https://doi.org/10.1016/j.jhazmat.2020.124102.

[13] J. Margot, L. Rossi, D.A. Barry, C. Holliger, A review of the fate of micropollutants in wastewater treatment plants, WIREs. Water. 2 (5) (2015) 457–487, https://doi.org/10.1002/wat2.1090.

[14] G. Hancu, D. Lupu, A. Milan, M. Budău, E. Barabás-Hajdu, Enantioselective analysis of venlafaxine and its active metabolites: a review on the separation methodologies, Biomed. Chromatogr. 35 (1) (2021) e4874, https://doi.org/10.1002/bmc.4874.

[15] T.T.T. Tran, D.M. Nguyen, A.Q. Dao, V.T. Le, Y. Vasseghian, A state-of-the-art review on the nanomaterial-based sensor for detection of venlafaxine, Chemosphere 297 (2022) 134116, https://doi.org/10.1016/j.chemosphere.2022.134116.

[16] S. Tajik, H. Beitollahi, Z. Dourandish, K. Zhang, Q.V. Le, T.P. Nguyen, S.Y. Kim, M. Shokouhimehr, Recent advances in the electrochemical sensing of venlafaxine: an antidepressant drug and environmental contaminant, Sensors 20 (13) (2020) 3675, https://doi.org/10.3390/s20133675.

[17] M. Rizk, E.A. Taha, M.M.A. El-Alamin, H.A.M. Hendawy, Y.M. Sayed, Highly sensitive carbon based sensors using zinc oxide nanoparticles immobilized multiwalled carbon nanotubes for simultaneous determination of desvenlafaxine succinate and clonazepam, J. Electrochem. Soc. 165 (7) (2018) H333, https://doi.org/10.1149/2.0551807jes.

[18] B.J. Sanghavi, A.K. Srivastava, Adsorptive stripping differential pulse voltammetric determination of venlafaxine and desvenlafaxine employing Nafion–carbon nanotube composite glassy carbon electrode, Electrochim. Acta 56 (11) (2011) 4188–4196, https://doi.org/10.1016/j.electacta.2011.01.097.

[19] B. Maddah, M. Cheraghveisi, M. Najafi, Developing a modified electrode based on La^{3+}/Co_3O_4 nanocubes and its usage to electrochemical detection of venlafaxine, Int. J. Environ. Anal. Chem. 100 (2) (2020) 121–133, https://doi.org/10.1080/03067319.2019.1631303.

[20] H. Beitollahi, S. Jahani, S. Tajik, M.R. Ganjali, F. Faridbod, T. Alizadeh, Voltammetric determination of venlafaxine as an antidepressant drug employing Gd_2O_3 nanoparticles graphite screen printed electrode, J. Rare Earth 37 (3) (2019) 322–328, https://doi.org/10.1016/j.jre.2018.09.001.

[21] S. Baluchová, A. Daňhel, H. Dejmková, V. Ostatná, M. Fojta, K. Schwarzová-Pecková, Recent progress in the applications of boron doped diamond electrodes in electroanalysis of organic compounds and biomolecules – A review, Anal. Chim. Acta 1077 (2019) 30–66, https://doi.org/10.1016/j.aca.2019.05.041.

[22] J.V. Macpherson, A practical guide to using boron doped diamond in electrochemical research, Phys. Chem. Chem. Phys. 17 (5) (2015) 2935–2949, https://doi.org/10.1039/C4CP04022H.

[23] K. Schwarzová-Pecková, J. Vosáhlová, J. Barek, I. Šloufová, E. Pavlova, V. Petrák, J. Zavázalová, Influence of boron content on the morphological, spectral, and electroanalytical characteristics of anodically oxidized boron-doped diamond electrodes, Electrochim. Acta 243 (2017) 170–182, https://doi.org/10.1016/j.electacta.2017.05.006.

[24] S. Baluchová, A. Taylor, V. Mortet, S. Sedláková, L. Klimša, J. Kopeček, O. Hák, K. Schwarzová-Pecková, Porous boron doped diamond for dopamine sensing: effect of boron doping level on morphology and electrochemical performance, Electrochim. Acta 327 (2019) 135025, https://doi.org/10.1016/j.electacta.2019.135025.

[25] P. Čambal, S. Baluchová, A. Taylor, L. Míka, M. Vondráček, Z. Gedeonová, P. Hubík, V. Mortet, K. Schwarzová-Pecková, Boron-doped {113}, {115} and {118}-oriented single-crystal diamond electrodes: effect of surface pre-treatment, Electrochim. Acta 469 (2023) 143214, https://doi.org/10.1016/j.electacta.2023.143214.

[26] S. Baluchová, A. Mamaloukou, R.H.J.M. Koldenhof, J.G. Buijnsters, Modification-free boron-doped diamond as a sensing material for direct and reliable detection of the antiretroviral drug nevirapine, Electrochim. Acta 450 (2023) 142238, https://doi.org/10.1016/j.electacta.2023.142238.

[27] T.A. Ivandini, T. Watanabe, T. Matsui, Y. Ootani, S. Iizuka, R. Toyoshima, H. Kodama, H. Kondoh, Y. Tateyama, Y. Einaga, Influence of surface orientation on electrochemical properties of boron-doped diamond, J. Phys. Chem. C 123 (9) (2019) 5336–5344, https://doi.org/10.1021/acs.jpcc.8b10406.

[28] Z. Liu, A.F. Sartori, J.G. Buijnsters, Role of sp2 carbon in non-enzymatic electrochemical sensing of glucose using boron-doped diamond electrodes, Electrochem. Commun. 130 (2021) 107096, https://doi.org/10.1016/j.elecom.2021.107096.

[29] Z. Liu, S. Baluchová, Z. Li, Y. Gonzalez-Garcia, C.E. Hall, J.G. Buijnsters, Unravelling microstructure-electroactivity relationships in free-standing polycrystalline boron-doped diamond: a mapping study, Acta Mater. 266 (2024) 119671, https://doi.org/10.1016/j.actamat.2024.119671.

[30] S. Feijoo, S. Baluchová, M. Kamali, J.G. Buijnsters, R. Dewil, Single-crystal vs polycrystalline boron-doped diamond anodes: comparing degradation efficiencies of carbamazepine in electrochemical water treatment, Environ. Pollut. 347 (2024) 123705, https://doi.org/10.1016/j.envpol.2024.123705.

[31] C.P. Sousa, F.W.P. Ribeiro, T.M.B.F. Oliveira, G.R. Salazar-Banda, P. de Lima-Neto, S. Morais, A.N. Correia, Electroanalysis of pharmaceuticals on boron-doped diamond electrodes: a review, ChemElectroChem. 6 (9) (2019) 2350–2378, https://doi.org/10.1002/celc.201801742.

[32] M. Yence, A. Cetinkaya, G. Ozcelikay, S.I. Kaya, S.A. Ozkan, Boron-doped diamond electrodes: recent developments and advances in view of electrochemical drug sensors, Crit. Rev. Anal. Chem. 52 (5) (2022) 1122–1138, https://doi.org/10.1080/10408347.2020.1863769.

[33] R. Silva Mariano, B. Coldibeli, G. Scalianti Ceravolo, E. Romão Sartori, Ultra-sensitive determination of serotonergic antidepressant vortioxetine in pharmaceutical and blood samples at the boron-doped diamond electrode, J. Electroanal. Chem. 952 (2024) 117962, https://doi.org/10.1016/j.jelechem.2023.117962.

[34] S.N. Samanci, G. Ozcelikay-Akyildiz, E.B. Atici, S.A. Ozkan, Electrochemical behaviour and determination of niraparib using glassy carbon and boron-doped diamond electrodes, Diam. Relat. Mater. 152 (2025) 111964, https://doi.org/10.1016/j.diamond.2025.111964.

[35] A. Cardoso, A.C. Maia Fraga, M. da Silva Araujo, R. de Matos, C.R. Teixeira Tarley, C.S. Ripke Ferreira, O.O. Santos, R.A. Medeiros, Innovation in venlafaxine detection: development and application of electroanalytical method using a boron-doped diamond electrode and performance comparison with UHPLC-MS/MS, Talanta 293 (2025) 127988, https://doi.org/10.1016/j.talanta.2025.127988.

[36] F.C. Moreira, R.A.R. Boaventura, E. Brillas, V.J.P. Vilar, Electrochemical advanced oxidation processes: a review on their application to synthetic and real wastewaters, Appl. Catal. B: Environ. 202 (2017) 217–261, https://doi.org/10.1016/j.apcatb.2016.08.037.

[37] S.O. Ganiyu, C.A. Martínez-Huitle, M.A. Oturan, Electrochemical advanced oxidation processes for wastewater treatment: advances in formation and detection of reactive species and mechanisms, Cur. Opin. Electrochem. 27 (2021) 100678, https://doi.org/10.1016/j.coelec.2020.100678.

[38] S. Garcia-Segura, J.D. Ocon, M.N. Chong, Electrochemical oxidation remediation of real wastewater effluents — a review, Process. Saf. Environ. Prot. 113 (2018) 48–67, https://doi.org/10.1016/j.psep.2017.09.014.

[39] K.N. de Oliveira Silva, M.A. Rodrigo, E.V. dos Santos, Electrochemical treatment of soil-washing effluent with boron-doped diamond electrodes: a review, Curr. Opin.

Solid State Mater. Sci. 25 (6) (2021) 100962, https://doi.org/10.1016/j.cossms.2021.100962.
[40] A.V. Karim, P.V. Nidheesh, M.A. Oturan, Boron-doped diamond electrodes for the mineralization of organic pollutants in the real wastewater, Cur. Opin. Electrochem. 30 (2021) 100855, https://doi.org/10.1016/j.coelec.2021.100855.
[41] D. Suresh Babu, J.M.C. Mol, J.G. Buijnsters, Experimental insights into anodic oxidation of hexafluoropropylene oxide dimer acid (GenX) on boron-doped diamond anodes, Chemosphere 288 (2022) 132417, https://doi.org/10.1016/j.chemosphere.2021.132417.
[42] R.C.P. Oliveira, J.G. Buijnsters, M.M. Mateus, J.C.M. Bordado, D.M.F. Santos, On the electrooxidation of kraft black liquor on boron-doped diamond, J. Electroanal. Chem. 909 (2022) 116151, https://doi.org/10.1016/j.jelechem.2022.116151.
[43] L. Pražáková, J. Fischer, A. Taylor, A. Kubíčková, Boron-doped diamond electrodes: examining the effect of doping level on the degradation of pharmaceuticals, Mon. Chem. 155 (8) (2024) 845–850, https://doi.org/10.1007/s00706-024-03233-0.
[44] E. Mordačíková, M. Vojs, K. Grabicová, M. Marton, P. Michniak, V. Řeháček, A. Bořík, R. Grabic, J. Bruncko, T. Mackuľak, A. Vojs Staňová, Influence of boron doped diamond electrodes properties on the elimination of selected pharmaceuticals from wastewater, J. Electroanal. Chem. 862 (2020) 114007, https://doi.org/10.1016/j.jelechem.2020.114007.
[45] S. Garcia-Segura, E. Vieira dos Santos, C.A. Martínez-Huitle, Role of sp3/sp2 ratio on the electrocatalytic properties of boron-doped diamond electrodes: a mini review, Electrochem. Commun. 59 (2015) 52–55, https://doi.org/10.1016/j.elecom.2015.07.002.
[46] B. Yu, Q. Han, C. Li, Y. Zhu, X. Jin, Z. Dai, Influencing factors of venlafaxine degradation at boron-doped diamond anode, Arab. J. Chem. 15 (1) (2022) 103463, https://doi.org/10.1016/j.arabjc.2021.103463.
[47] R. Granados-Fernández, C.P. Navarro-Cacho, C.M. Fernández-Marchante, J. Lobato, M.A. Rodrigo, On the manufacturing of tailored electrochemical cells using 3-D printing technology: a case study, Chem. Eng. J. 496 (2024) 153765, https://doi.org/10.1016/j.cej.2024.153765.
[48] E.M. Richter, D.P. Rocha, R.M. Cardoso, E.M. Keefe, C.W. Foster, R.A.A. Munoz, C. E. Banks, Complete additively manufactured (3D-printed) electrochemical sensing platform, Anal. Chem. 91 (20) (2019) 12844–12851, https://doi.org/10.1021/acs.analchem.9b02573.
[49] T. Sebechlebská, E. Vaněčková, M.K. Choińska-Młynarczyk, T. Navrátil, L. Poltorak, A. Bonini, F. Vivaldi, V. Kolivoška, 3D printed platform for impedimetric sensing of liquids and microfluidic channels, Anal. Chem. 94 (41) (2022) 14426–14433, https://doi.org/10.1021/acs.analchem.2c03191.
[50] R.A. Márquez-Montes, V.H. Collins-Martínez, I. Pérez-Reyes, D. Chávez-Flores, O. A. Graeve, V.H. Ramos-Sánchez, Electrochemical engineering assessment of a novel 3D-printed filter-press electrochemical reactor for multipurpose laboratory applications, ACS Sustain. Chem. Eng. 8 (9) (2020) 3896–3905, https://doi.org/10.1021/acssuschemeng.9b07368.
[51] L.A. Hutton, J.G. Iacobini, E. Bitziou, R.B. Channon, M.E. Newton, J. V. Macpherson, Examination of the factors affecting the electrochemical performance of oxygen-terminated polycrystalline boron-doped diamond electrodes, Anal. Chem. 85 (15) (2013) 7230–7240, https://doi.org/10.1021/ac401042t.
[52] G.F. Pereira, L.S. Andrade, R.C. Rocha-Filho, N. Bocchi, S.R. Biaggio, Electrochemical determination of bisphenol A using a boron-doped diamond electrode, Electrochim. Acta 82 (2012) 3–8, https://doi.org/10.1016/j.electacta.2012.03.157.
[53] H.B. Suffredini, V.A. Pedrosa, L. Codognoto, S.A.S. Machado, R.C. Rocha-Filho, L. A. Avaca, Enhanced electrochemical response of boron-doped diamond electrodes brought on by a cathodic surface pre-treatment, Electrochim. Acta 49 (22) (2004) 4021–4026, https://doi.org/10.1016/j.electacta.2004.01.082.
[54] R.A. Medeiros, R.C. Rocha-Filho, O. Fatibello-Filho, Simultaneous voltammetric determination of phenolic antioxidants in food using a boron-doped diamond electrode, Food Chem. 123 (3) (2010) 886–891, https://doi.org/10.1016/j.foodchem.2010.05.010.
[55] M.F.B. Ali, M.R. El-Zahry, A comparative study of different electrodeposited $NiCo_2O_4$ microspheres anchored on a reduced graphene oxide platform: electrochemical sensor for anti-depressant drug venlafaxine, RSC. Adv. 9 (54) (2019) 31609–31620, https://doi.org/10.1039/C9RA04999A.
[56] Z. Dourandish, H. Beitollahi, I. Sheikhshoaie, Simultaneous voltammetric determination of epinine and venlafaxine using disposable screen-printed graphite electrode modified by bimetallic Ni-Co-metal–organic-framework nanosheets, Molecules. (5) (2023) 28, https://doi.org/10.3390/molecules28052128.
[57] P. Mohammadzadeh Jahani, H. Akbari Javar, H. Mahmoudi-Moghaddam, A new electrochemical sensor based on europium-doped NiO nanocomposite for detection of venlafaxine, Measurement 173 (2021) 108616, https://doi.org/10.1016/j.measurement.2020.108616.
[58] S.Z. Mohammadi, S. Tajik, F. Mousazadeh, Y. Neiestani, Constructing a simple and sensitive electrochemical sensor for the determination of venlafaxine based on Fe_3O_4@SiO_2/MWCNT nanocomposite-modified screen-printed electrode, J. Mater. Sci.: Mater. Electron. 34 (22) (2023) 1641, https://doi.org/10.1007/s10854-023-11030-4.
[59] M.A. Bajaber, A.H. Kamel, All-solid state potentiometric sensors for desvenlafaxine detection using biomimetic imprinted polymers as recognition receptors, Polymers. (Basel) 14 (22) (2022) 4814, https://doi.org/10.3390/polym14224814.
[60] R.T. Elbahy, G.M. El-Sayed, S.S. Abbas, R.M. Arafa, In-line white quantification of desvenlafaxine succinate by glassy carbon sensor decorated with multi-walled carbon nanotubes in its pharmaceutical form and biological matrices, Microchem. J. 204 (2024) 111066, https://doi.org/10.1016/j.microc.2024.111066.
[61] S. Baluchová, J. Barek, L.I.N. Tomé, C.M.A. Brett, K. Schwarzová-Pecková, Vanillylmandelic and homovanillic acid: electroanalysis at non-modified and polymer-modified carbon-based electrodes, J. Electroanal. Chem. 821 (2018) 22–32, https://doi.org/10.1016/j.jelechem.2018.03.011.
[62] M. Narmadha, M. Noel, V. Suryanarayanan, Relative deactivation of boron-doped diamond (BDD) and glassy carbon (GC) electrodes in different electrolyte media containing substituted phenols – Voltammetric and surface morphologic studies, J. Electroanal. Chem. 655 (2) (2011) 103–110, https://doi.org/10.1016/j.jelechem.2011.03.003.
[63] L. Janíková, J. Chýlková, R. Šelešovská, M. Sedlák, J. Váňa, L. Dušek, J. Bartáček, Electrochemical behavior of plant growth stimulator 1-naphthaleneacetic acid and its voltammetric determination using boron doped diamond electrode, J. Electroanal. Chem. 859 (2020) 113855, https://doi.org/10.1016/j.jelechem.2020.113855.
[64] S. Lü, Voltammetric determination of 1-naphthylacetic acid in soil samples using carbon nanotubes film modified electrode, Anal. Lett. 36 (8) (2003) 1523–1534, https://doi.org/10.1081/AL-120021534.
[65] C.Q. Duan, Y.M. Zhang, Z.N. Gao, Electrochemical behaviors and electrochemical determination of 1-naphthaleneacetic acid at an ionic liquid modified carbon paste electrode, Croat. Chem. Acta 85 (1) (2012) 27–32, https://doi.org/10.5562/cca1901.
[66] J. Vosáhlová, J. Sochr, S. Baluchová, Ľ. Švorc, A. Taylor, K. Schwarzová-Pecková, Comparison of carbon-based electrodes for detection of cresols in voltammetry and HPLC with electrochemical detection, Electroanalysis. 32 (10) (2020) 2193–2204, https://doi.org/10.1002/elan.202060103.
[67] M. Ferreira, H. Varela, R.M. Torresi, G. Tremiliosi-Filho, Electrode passivation caused by polymerization of different phenolic compounds, Electrochim. Acta 52 (2) (2006) 434–442, https://doi.org/10.1016/j.electacta.2006.05.025.
[68] S.B. Gomes Junior, N.S. Conceição, G.F.S. dos Santos, J.G.A. Rodrigues, W. Romão, R.Q. Ferreira, Determination of benzoylecgonine in synthetic urine samples via square-wave voltammetry with boron-doped diamond electrode, J. Solid State Electrochem. 29 (3) (2025) 1205–1215, https://doi.org/10.1007/s10008-024-05922-6.
[69] S. Sultan, A. Shah, N. Firdous, J. Nisar, M.N. Ashiq, I. Shah, A novel electrochemical sensing platform for the detection of the antidepressant drug, venlafaxine, in water and biological specimens, Chemosensors 10 (10) (2022), https://doi.org/10.3390/chemosensors10100400.
[70] X.M. Lense, C. Hiemke, C.S.M. Funk, U. Havemann-Reinecke, G. Hefner, A. Menke, R. Mössner, T.G. Riemer, M. Scherf-Clavel, G. Schoretsanitis, et al., Venlafaxine's therapeutic reference range in the treatment of depression revised: a systematic review and meta-analysis, Psychopharmacology (Berl.) 241 (2) (2024) 275–289, https://doi.org/10.1007/s00213-023-06484-7.
[71] A.F. Hagel, H. Albrecht, W. Dauth, W. Hagel, F. Vitali, I. Ganzleben, H.W. Schultis, P.C. Konturek, J. Stein, M.F. Neurath, M. Raithel, Plasma concentrations of ascorbic acid in a cross section of the German population, J. Int. Med. Res. 46 (1) (2017) 168–174, https://doi.org/10.1177/0300060517714387.
[72] G. Divyapriya, P.V. Nidheesh, Electrochemically generated sulfate radicals by boron doped diamond and its environmental applications, Curr. Opin. Solid State Mater. Sci. 25 (3) (2021) 100921, https://doi.org/10.1016/j.cossms.2021.100921.
[73] M. Amerio-Cox, J.J. Tully, F. Tang, A. Dettlaff, J.V. Macpherson, T. Mollart, T. Sidnell, S. Mathias, P. Sears, M.J. Bussemaker, Investigation of short chain PFAS degradation efficiency using free-standing boron doped diamond electrodes at high current density in a flow cell, ACS Electrochem 1 (10) (2025) 2014–2023, https://doi.org/10.1021/acselectrochem.5c00121.
[74] E. Brillas, I. Sirés, M.A. Oturan, Electro-Fenton process and related electrochemical technologies based on Fenton's reaction chemistry, Chem. Rev. 109 (12) (2009) 6570–6631, https://doi.org/10.1021/cr900136g.
[75] C. Comninellis, Electrocatalysis in the electrochemical conversion/combustion of organic pollutants for waste water treatment, Electrochim. Acta 39 (11) (1994) 1857–1862, https://doi.org/10.1016/0013-4686(94)85175-1.
[76] A.J. Lucio, J.V. Macpherson, Combined voltammetric measurement of pH and free chlorine speciation using a micro-spot sp^2 bonded carbon–boron doped diamond electrode, Anal. Chem. 92 (24) (2020) 16072–16078, https://doi.org/10.1021/acs.analchem.0c03692.
[77] J. Hrabovsky, M. Zelensky, J. Sladek, M. Zukerstein, J. Fischer, K. Schwarzova-Peckova, A. Taylor, M. Veis, S. Mandal, O.A. Williams, N.M. Bulgakova, Laser-patterned boron-doped diamond electrodes with precise control of sp^2/sp^3 carbon lateral distribution, Appl. Surf. Sci. 639 (2023) 158268, https://doi.org/10.1016/j.apsusc.2023.158268.